GBA1 MUTATIONS ALTER THE PHENOTYPE AND BEHAVIOUR OF DOPAMINERGIC NEURONS IN PARKINSON´S DISEASE, INFLUENCING *VGLUT2* AND *CRYAB* EXPRESSION

Eva Rodríguez-Traver[1,2], Luz M. Suárez[1,2,4*], Carlos Crespo[3*], Irene González-Burgos[1,2*], Rebeca Vecino[1,2], Juan C. Jurado-Coronel[1], María Galán[1], Marta González-González[1], Rosario Moratalla[1,2, &], Carlos Vicario[1,2,&, #]

[1]Instituto Cajal, Consejo Superior de Investigaciones Científicas (CSIC), Madrid, Spain; [2]CIBERNED, Instituto de Salud Carlos III (ISCIII), Madrid, Spain; [3]Departamento de Biología Celular, Estructura de Investigación Interdisciplinar en Biotecnología y Biomedicina (BIOTECMED), Universitat de Valencia, Valencia, Spain.

[4]Present address: Departamento de Genética, Fisiología y Microbiología. Facultad de Ciencias Biológicas, Universidad Complutense de Madrid, Spain.

[#]**Corresponding author**: Carlos Vicario, Instituto Cajal-CSIC, Avenida Doctor Arce 37, E-28002 Madrid, Spain. Email: cvicario@cajal.csic.es; Phone: (+34) 91-585-4721; Fax: (+34) 91-585-4754

[*]Luz M. Suárez, Carlos Crespo, and Irene González-Burgos contributed equally to this article.

[&]Carlos Vicario and Rosario Moratalla contributed equally to this article.

ABSTRACT

Mutations in the *glucocerebrosidase 1* (*GBA1*) gene, encoding a lysosomal enzyme, are major risk factors for Parkinson´s disease (PD). The impact of *GBA1* mutations on neuronal maturation, function and degeneration was investigated in dopaminergic (DA) neurons obtained from our repository of induced pluripotent stem cells (iPS cells or iPSCs), cells derived from PD patients carrying the heterozygous N370S or L444P mutation in *GBA1*, or from healthy subjects (controls). DA neurons co-expressing TH and VGLUT2 were detected in the cultures, and their number and/or expression of *SLC17A6/VGLUT2* mRNA was markedly reduced in both N370S and L444P cultures. Electrophysiological recordings revealed a significant increase in the firing rate of N370S but not L444P neurons, whereas evoked dopamine release was stronger from neurons carrying either mutation than from the controls. Remarkably, neurons carrying either *GBA1* mutation accumulated abundant degenerative bodies, multilamellar bodies, autophagosomes and Golgi apparatus vacuolated dictyosomes, with some differences in neurons carrying the N370S or L444P mutation. Furthermore, there was a significant accumulation of α-synuclein aggregates in the cell body and dendrites of N370S neurons. Notably, a significant upregulation of the small chaperone *CRYAB* (HSPB5/alpha-crystallin-B) was found early in DA neuron differentiation and in the Substantia Nigra of PD patients. Our findings indicate that N370S and L444P *GBA1* mutations produce some similar and other distinct molecular, electrical and ultrastructural alterations in DA neurons. They suggest that these mutations impair the VGLUT2 subpopulation of midbrain DA neurons, and provoke stress responses early in the neuronal differentiation programme.

Key words: Parkinson's disease, *GBA1*, iPSC, dopaminergic neuron, VGLUT2, degenerative body; multilamellar body, α-synuclein, synaptic activity, CRYAB.

INTRODUCTION

The *GBA1* gene encodes the lysosomal enzyme β-glucocerebrosidase 1 (glucosylceramidase beta, GCase1), which catalyzes the hydrolysis of glucosylceramide (glucocerebroside or GlcCer) to ceramide and glucose, and that of glucosylsphingomyelin. Mutations in *GBA1* are among the strongest genetic risk factors for Parkinson´s disease (PD).[1-10] Around 350 different mutations in *GBA1* have been reported but the heterozygous N370S and L444P are those most frequently found in PD patients. *GBA1* mutations have been estimated to increase the risk of PD 5- to 20-fold, while 5-25% of PD cases carry a mutation in this gene.[4,5,7,11-14] Although *GBA1*-associated PD (*GBA1*-PD) has similar symptomatology to idiopathic PD, *GBA1* mutations favor an earlier onset of the disease, and a higher frequency of cognitive impairment and dementia.[5,6,11,15-18] Importantly, the brains of idiopathic PD patients without *GBA1* mutations have less GCase and weaker GCase activity, probably due to the deleterious effect of aggregated α-synuclein (α-syn), a major component of Lewy bodies, on the enzyme.[5,19-23]

Discrepancies regarding GlcCer accumulation have been observed in different brain regions *in vivo.*[10] Thus, no GlcCer accumulation was evident in putamen and cerebellum samples from *GBA1*-PD patients,[24] whereas there was a significant increase in GlCer and glucosylsphingosine (GluSph) in the hippocampus and substantia nigra of idiopathic PD patients.[25]

The molecular mechanisms that link the alterations to GCase1 protein structure and activity due to *GBA1* mutations with an increased risk of PD are still not fully understood. Several hypotheses have been proposed that associate GCase1 deficiency with α-syn aggregation. Firstly, a deficiency in GCase would

lead to the accumulation of GlcCer in the lysosome, which could in turn perturb lipid homeostasis and affect α-syn clearance. This would stabilize α-syn oligomers, promoting the formation and accumulation of insoluble α-syn fibrils that would impair GCase trafficking from the endoplasmic reticulum (ER) to the Golgi apparatus (GA), further reducing enzyme activity in the lysosome.[4,14,20,26-28] Elsewhere, a direct interaction between GluCer and α-syn has been suggested that would lead to protein aggregation.[27] In fact, mutated GCase1 has been seen to co-localize with α-syn in lysosomes, Lewy bodies and neurites.[29] Alternatively, reducing GCase activity may exacerbate pre-existing α-syn aggregation and hence, the pathological susceptibility of neurons.[30] Moreover, it was recently proposed that α-syn degradation could be impaired by mutant GCase, leading to α-syn accumulation. Indeed, GCase misfolding in the ER leads to a loss of enzymatic activity that impedes α-syn degradation, which could drive the degeneration and death of DA neurons due to lysosomal-autophagic dysfunction.[31] Along similar lines, recent evidence indicates that *GBA1* mutations impair α-syn degradation by inhibiting chaperone-mediated autophagy (CMA).[32]

Thus, misfolded GCase alone, or in combination with α-syn aggregation, can generate dysfunctional phenotypes in the cells, inducing ER stress, activation of the unfolded protein response (UPR), lysosome and autophagic dysfunction, cholesterol accumulation, mitochondrial dysfunction, reactive oxygen species (ROS) production and defects in calcium homeostasis.[2,6,20,27,28,31,33-42] All these findings illustrate the progress made in understanding the cellular and molecular mechanisms leading to cellular dysfunction and neuronal degeneration in *GBA1*-PD.

However, important questions remain to be addressed in order to gain a deeper understanding of the relationship between impaired GCase and PD etiopathology, which could shed light on potential treatments to slow or impede disease progression. Among other questions, this includes the neuronal differentiation and maturation stage when the first alterations triggered by *GBA1* mutations are observed. Moreover, it is unclear to what extent the heterozygous N370S and L444P mutations in *GBA1* trigger similar or distinct alterations in neurons. Here we identified common and distinct functional impairments in iPSC-DA neurons carrying N370S or L444P *GBA1* mutations, as well as other degeneration related effects. Importantly, some of these alterations appear in relatively immature DA neurons, such as reduced VGLUT2 and increased CRYAB expression, suggesting that they may potentially serve as molecular targets and biomarkers in *GBA1*-PD.

MATERIALS AND METHODS

Differentiation of human iPSCs (hiPSCs) into DA neurons

The vector-free hiPSCs used in this study were generated and characterized previously in our laboratory,[12,13,43] and they have been deposited in the Spanish National Stem Cell Bank/Banco Nacional de Líneas Celulares (BNLC, Instituto de Salud Carlos III, Spain).

To differentiate the hiPSCs into DA neurons, we designed a protocol based on previous publications.[44-46] First, the hiPSC colonies grown on mouse embryonic fibroblasts (MEFs) were dissociated into a single cell suspension by incubating them with accutase for 15-25 minutes at 37 ºC in an atmosphere of 5% CO_2. As this treatment also dissociates the MEFs, the cell suspension recovered was

plated on 0.1% gelatin-coated culture dishes and left for 1.5 hours. After this period the MEFs had adhered to the gelatin, the supernatant containing the hiPSCs could be collected and the cells recovered by centrifugation for 5 minutes at 200g. In a pilot study, this supernatant was then seeded on coated Thermanox plastic coverslips and the cells were immunostained with antibodies against NANOG to ensure the purity of the hiPSC preparation. For differentiation, the pellet of hiPSC was resuspended in MEF-conditioned hiPSC medium supplemented with FGF-2 (6 ng/mL) and Y-27632 (10 μM). The cell suspensions were plated on vitronectin-coated culture dishes at a density of 50,000-80,000 cells/cm^2, and the medium was changed every other day using MEF-conditioned hiPSC medium supplemented with FGF-2.

Once the cultures reached a cell confluence of 90-100%, neural induction commenced by changing the medium to hiPSC medium supplemented with Noggin (250 ng/mL, day 0), containing A83-01 (5 μM) or SB431542 (10 μM). The medium was changed on day 1 of the culture to hiPSC medium supplemented with Noggin, A83, Sonic Hedgehog C25II (SHH, 100 ng/mL: R&D Systems, RYD-464-SH-025), Purmorphamine (2 μM: Miltenyi Biotec, 130-104-465) and FGF-8 (100 ng/mL: Peprotech,100-25B). On day 3, CHIR99021 (CHIR, 3 μM: Miltenyi Biotec, 130-103-926) was also added along with the factors added on day 1. From day 5 to day 9, the hiPSC medium was incrementally shifted to DMEMF12N2 medium (25%, 50%, 75%) every 2 days, and on day 7 and 9 the medium was only supplemented with Noggin and CHIR. On day 11, the medium was changed to Neurobasal/B27/GlutaMax supplemented with CHIR and with BDNF (20 ng/mL), ascorbic acid (0.2 mM), GDNF (20 ng/mL), dibutyril cAMP (0.5 mM) and TGFβ3 (1 ng/mL: BAGCT

compounds). From day 13, CHIR was no longer added, BAGCT was included and the medium was changed every other day until the cells were dissociated with accutase and collected on days 17-20 (depending on the confluence of the cultures). The cells recovered were then plated on coverslips in the wells of 24 multi-well plates, or on 48, 12 or 6 multi-well plates without coverslips or on a layer of mouse astrocytes (see below). Before plating, both the coverslips and wells were coated with different combinations of molecules (including poly-ornithine, poly-D-lysine, fibronectin, laminin or matrigel) to ensure the best attachment and the differentiation-maturation of neurons. No clear differences in the number of neurons were observed between the different coatings and therefore, all the results obtained were combined.

For long-term maturation studies, cells were plated on a layer of mitotically inactivated primary astrocytes obtained from the cerebral cortex of postnatal day 0-2 (P0-P2) C57Bl/6 mice (kindly donated by Drs I. Torres-Alemán, L.M. García-Segura, and M.A. Arévalo, Cajal Institute, Madrid, Spain). The astrocytes were plated at 50,000-65,000 cells/cm^2 on poly-lysine-coated coverslips in DMEM containing 10% foetal bovine serum (FBS) and when confluent they were treated with cytosine-β-D-arabinofuranoside (AraC, 10 μM) for 2-3 days. The AraC was then removed and washed out with fresh medium.

The hiPSC-derived cells were collected, as mentioned above, resuspended in Neurobasal/B27/GlutaMax with BAGCT, and plated at 300,000-400,000 cells/cm^2 on coated coverslips and wells or at 200,000 cells/cm^2 on astrocytes. Depending on the studies carried out, the cells were maintained in culture from 18 to 104 days, changing the medium containing BAGCT every 2-3 days.

Control, *N370S-GBA1* and *L444P-GBA*1 hiPSCs were always differentiated in parallel, and similarly, all the assays and analyses were performed in parallel.

The protocol using Noggin and A83-01 (5 μM) or Noggin and SB431542 (10 μM) favoured the production of tyrosine hydroxylase (TH)$^+$ neurons and the relatively stronger expression of mRNAs encoding dopaminergic transcripts (such as *TH*, *FOXA2*, *NURR1*, *LMX1A* and *LMX1B*) than other combination tested, including: LDN193189 (100 nM) and SB431542 (10 μM) or LDN193189 (100 nM) and A83-01 (5 μM). The proportion of neurons obtained after 30-33 DIV when LDN/SB, or LDN/A83 were used was very similar: 34.8% (±2.3%) of (β-III-Tubulin$^+$ or TUJ1$^+$ cells) cells were TH$^+$ (n=13), while 16.6% (±1.1%) of the total number of cells were TUJ1$^+$ and 6.1% (±0.1%) were TH$^+$. By contrast, adding Noggin/A83 or Noggin/SB, increased the proportion of TUJ1$^+$ and TH$^+$ neurons: 56.7% (±2.8%) of the TUJ1$^+$ cells were TH$^+$, and 33.5% (±3.0%) of the total cell population were TUJ1$^+$ and 18.3% (±1.4%) were TH$^+$. Noggin/A83 or Noggin/SB in fewer experiments, together with SHH, Pur, FGF8 and CHIR99021, were the molecules chosen to induce hiPSC differentiation into a midbrain dopaminergic cell fate.

Real-Time Quantitative Reverse Transcription Polymerase Chain Reaction (RT-qPCR)

After removing the medium, the cells were lysed in RA1/β-mercaptoethanol buffer and the extract was collected and immediately frozen in liquid nitrogen and stored at -80 ºC. The NucleoSpin RNA extraction kit (Macherey-Nagel, Cat. No. 740955.50) was used to purify the RNA from the cells, according to the manufacturer's instructions. The concentration and quality of the RNA was

determined using NanoDrop One (Thermo Scientific, ND-ONE-W): absorbance ratios A260/280 >1.8 and A260/230 >1.5.

Complementary DNA (cDNA) was obtained by reverse transcription of 250-500 ng of the initial RNA using the SuperScript III enzyme (Invitrogen), according to the manufacturer's instructions and our protocols.[47] To determine the relative expression of different genes the RT-qPCR analysis was performed in triplicate using Power SYBR Green or Power SYBR Green Fast with the appropriate negative controls (one negative control containing water instead of cDNA and a second, in which the negative control for the reverse transcriptase reaction was added instead of cDNA). The primer pairs, designed with either Lasergene software or purchased directly (Supplementary Table 1), were added to the SYBR Green mix, which was then added to each well of a 96 well-plate for RT-qPCR. Subsequently, the cDNA was added to each well and the plate was inserted into one of two RT-qPCR thermocyclers: 7500 Fast Real-Time PCR and QuantStudio 3 (Applied Biosystems), which use 7500 Software v2.3 and software QuantStudioTM Design & Analysis, respectively. All the RT-qPCR cDNA products obtained were sequenced to verify that they corresponded to the expected fragments.

For quantification, the Ct value for each target gene was normalized to the Ct value for *GAPDH* using the comparative C_T method with the equation $2^{-\Delta C_T}$.[48,49] This method was used for all the genes as the slope obtained after representing the C_T of each gene relative to that for *GAPDH* was between 0.1 and -0.1, indicating the efficiency of the qPCR reaction was the same for the gene studied and for *GAPDH*. Changes in gene expression were compared between the N370S/wt and L444P/wt cultures, and also with the expression in the control

(wt/wt) cultures, using the comparative C_T method with the equation $2^{-\Delta\Delta C_T}$. Values were obtained as the fold change on a log2 scale, and then represented using violin plots after conversion to a linear scale. Violin plots represent the density, distribution and the median of the data obtained from three differentiation experiments performed in triplicate. Statistical analysis was performed using an unpaired Student's t test, applying Welch's correction when the F-test indicated that the variances of both groups differed significantly.

Immunocytochemistry (ICC)

Cells were fixed for 25 minutes with 4% paraformaldehyde (PFA) and preserved at 4 ºC in sodium azide (0.02% in phosphate-buffered saline - PBS). For immunocytochemistry (ICC), cells were first washed three times with PBS and then incubated for 1 hour at room temperature (RmT) in permeabilization/blocking buffer (0.1-0.4% Triton X-100/Normal goat or donkey serum/PBS), prior to probing them 20-22 hours with primary antibodies against: CRYAB (1:250: Abcam Cat# ab76467, RRID:AB_1523120); FOXA2 (1:100: Abcam Cat# ab108422, RRID:AB_11157157); GABA (1:2000: Sigma Cat# A2051, RRID:AB_2314459); GIRK2 (1:200: Abcam Cat# ab65096, RRID:AB_1139732); MAP2 (1:250: Sigma-Aldrich Cat# M1406, RRID:AB_477171 and 1:1000: Synaptic Systems Cat# 188004, RRID:AB_2138181); α-synuclein LB509 (1:800: Abcam Cat# ab27766, RRID:AB_727020); TH (1:200: Millipore Cat# MAB318, RRID:AB_2201528 and 1:200: Millipore Cat# AB152, RRID:AB_390204); β-III-tubulin (TUJ1, 1:1000: Covance Cat# MMS-435P, RRID:AB_2313773 and TUJ1, 1:300: Abcam Cat# ab18207, RRID:AB_444319); VGLUT2 (1:500: Alomone Cat# AGC-036,

RRID:AB_2340950). Antibody binding was then detected with the appropriate secondary antibodies for 1 h at RmT, while the nuclei were stained with Hoechst. No specific signal was detected in the absence of the primary antibodies but in the presence of the secondary antibodies.

For quantification, confocal images from 5 or 10 random microscope fields were used per culture using a 63x objective or a 40x objective with a 1.5 zoom. Cells in the entire Z-stack were counted and the co-localization of specific markers was analysed in each individual Z-plane using ImageJ software (NIH, Bethesda, MD). The proportion of labelled cells was calculated relative to the total number of $MAP2^+$, $TUJ1^+$ or TH^+ neurons, or of the total Hoechst stained nuclei. The results were expressed as the mean ± S.E.M. of 3-33 cultures per genotype from 3-7 differentiation experiments. The specific n values for each ICC assay are given in the figure legends and the statistical analysis was carried out using one-way ANOVA followed by a Bonferrani or Tukey post-hoc test, or Kruskal-Wallis test followed by a Dunn post-hoc test.

Analysis of α-synuclein aggregates in DA neurons

The hiPSC-derived cells were fixed on DIV 95 or 103, treated for 1h with 0.1-0.2% Triton X-100/Normal goat serum(NGS)/PBS, and probed for 20-22 h at 4 ºC with antibodies against TH, MAP2 and α-syn. Cells were then washed with PBS and incubated with the appropriate secondary antibodies for 1h at RmT, washed and mounted with Mowiol after staining the nuclei with Hoechst. Confocal images (each containing a clearly defined TH^+ neuron) were obtained with a 63x objective using a 3.5 zoom. The neurons from wt/wt, N370S/wt and L444P/wt genotypes were analysed, and three images were taken from each

neuron: one from the soma and two from two dendrites. The number of α-syn aggregates was semi-automatically counted using ImageJ. First, a threshold for detecting TH^+ staining was set to detect the neuron of interest which was then manually traced and its somatic and dendritic area measured. Next, a threshold for α-syn^+ staining was applied to quantify the number of aggregates. This allowed for an automatic detection of aggregates above a specific threshold. The aggregates and areas were determined blind to the genotype, and expressed as the number of aggregates per somatic area or per dendritic area (in μm^2). Statistical analysis was performed using the non-parametric Kruskal-Wallis test followed by Dunn´s multiple comparisons test.

Dopamine release

Dopamine in the culture medium collected at 44, 51 and 59 DIV was assessed, and the results were combined in the analysis. To measure the basal dopamine, the culture medium was replaced with fresh medium for 24 hours before it was collected. Subsequently, fresh medium with KCl (56 mM) was added to the cells and after 20 min it was collected to measure the dopamine release evoked, while the cells were fixed with 4% PFA for TH ICC. All the supernatants were collected in the presence of EDTA (1 mM: Sigma-Aldrich, E5134) and sodium metabisulfite (4 mM: Sigma-Aldrich, S9000) to prevent dopamine degradation, and they were kept at -80 ºC. Dopamine was extracted and measured using the Dopamine Research Elisa™ assay kit, according to the manufacturer's instructions (Labor Diagnostika Nord GmbH & Co. KG). The final colorimetric reaction was monitored at 450 nm and the samples were quantified by comparing their absorbance to a reference curve prepared from known

dopamine concentrations (after subtracting the absorbance of the blank wells). The cross reactivity with other amines and with non-amine molecules in the assay was <0.007%-0.55% (according to the manufacturer´s information). Calculations were made following a non-linear regression for curve fitting using GraphPad Prism 5.0. Fixed cells were immunostained with an antibody against TH to determine the total number of TH^+ cells per well. For this, 10 fields per well (20x, 2-fold zoom or 10x, 4-fold zoom), were taken randomly following an established pattern. The total number of TH^+ cells per well was estimated as the number of TH^+ cells counted divided by 10 fields and then by the area of a field (to give the number of TH^+ neurons per μm^2), multiplied by the area of the well. The dopamine data was expressed as picograms (pg) of dopamine per TH^+ neuron, or as pg of dopamine per TH^+ neuron and per minute, as the mean (±S.E.M.) of 13-24 cultures per genotype and from 5 experiments. Statistical analysis was performed using one-way ANOVA with a Tukey post-hoc test.

Quantification of α-synuclein in the culture medium

The hiPSC derived neurons were maintained in culture for 47 or 89 DIV, when the medium was collected to determine the α-syn levels using the SimpleStep ELISA kits (Abcam ab210973 and ab 260052) according to the manufacturer´s instructions. No α-syn was detected in the α-syn knockout cells (according to the manufacturer), reflecting the specificity of this assay. The final colorimetric reaction was monitored at 450 nm and the samples were quantified by comparing their optical density (OD, after subtracting the OD of the blank wells) to a reference curve prepared from known concentrations of α-syn. Calculations followed a near-linear regression for fitting using GraphPad Prism 5.0 software

and fixed cells were immunostained with an antibody against TH to determine the total number of TH^+ cells per well, as described above. The data were expressed as picograms (pg/ml) of α-syn per TH^+ neuron and are the mean (±S.E.M.) of 16-19 cultures per genotype from 2 experiments. Statistical analysis was performed using one-way ANOVA with a Tukey post-hoc test.

Electrophysiology

Electrophysiological experiments were performed on hiPSC-differentiated neurons (82-93 DIV) cultured on a monolayer of mouse astrocytes growing on coverslips, which were transferred to a submersion-type recording chamber mounted on a DM6000FS Leica microscope. The chamber was continuously perfused (0.5 ml/min) with carbogen (95% O_2, 5% CO_2)-bubbled artificial cerebrospinal fluid (aCSF) at 36.5 ºC. The aCSF medium was prepared daily, with an osmolarity adjusted to 310 mOsm with sucrose and containing: 130 mM NaCl, 4 mM KCl, 2 mM $CaCl_2$, 1 mM $MgCl_2$, 10 mM HEPES, and 10 mM glucose [pH 7.4].

Whole-cell patch-clamp pipettes (borosilicate with filament, 1.5 mm outer diameter thick glass) were pulled on a Flamming/Brown micropipette puller P-97 (Sutter Instruments Co, Novato, CA) and had an initial resistance of 5–10 MΩ. The internal recording solution was adjusted to an osmolarity of 290 mOsm with sucrose and it contained (in mM): 130 mM Cs-gluconate, 10 mM NaCl, 2 mM $MgCl_2$, 0.2 mM EGTA, 1 mM NaATP, and 10 mM HEPES adjusted to pH 7.2. To visualize the cells, Alexa Fluor-488 hydrazide sodium salt (125 μM) was added to the internal solution.

Patch-clamp recordings were obtained in the whole-cell configuration using Axoclamp 2-B (Molecular Devices, Sunnyvale, CA, USA) and digitized at 3 KHz using 1440A Digidata (Molecular Devices). The amplifier bridge circuit was adjusted to compensate for serial resistance and monitored throughout the experiment. Passive properties (resting membrane potential -RMP, membrane capacitance -Cm, and membrane resistance -Rm) were analysed using the membrane test function integrated in the pClamp10 software. The intrinsic excitability was assessed in current clamp mode with a 500 ms somatic current injection and spontaneous synaptic activity was recorded holding the cells at -70 mV (voltage clamp). The data were stored and analysed on a digital system (pClamp v10.0, Molecular Devices). Results are presented as the mean (±S.E.M.) of 6-12 DA neurons (90-93 DIV) from two experiments. The data was analysed using one- or two-way ANOVA with a Dunn or Bonferroni post-test, respectively, or using the Chi-squared test, with $P<0.05$ considered significant.

Morphological analysis of the cells recorded

Neurons were injected with Alexa Fluor-488 while electrophysiological recordings were carried out (see above) and subsequently, they were fixed with 4% PFA and immunostained with antibodies against TH and MAP2. The samples were scanned using an AF 6000LX Leica microscope with a 20x objective to identify the Alexa Fluor 488 labelled cells. Once the recorded neurons had been recognized, they were imaged using a confocal microscope with a 40x objective and analysed using Fiji ImageJ software. The cells were first classified as TH^+ or TH^- and subsequently, TH^+ neurons were traced using ImageJ Sholl analysis software using the Bonfire program in MATLAB.[50] The

average length of the processes, their total length and the number of processes was also quantified. However, not all neurons recorded could be found on the coverslips after the electrophysiology experiments, probably because they died or because dye filling failed. Moreover, some TH^+ neurons were not completely filled with Alexa-488 and therefore, they were removed from the analysis.

In the Sholl analysis, the number of intersections depends on two factors, the genotype and the distance from the soma, such that a two-way ANOVA analysis with a Bonferroni´s test was performed. A one-way ANOVA with a Tukey´s post-test was used to analyse the length and number of processes per neuron. The results are expressed as the mean (±S.E.M.) of 8-9 neurons per genotype from 3 experiments.

Electron microscopy

The hiPSC-differentiated neurons (91-104 DIV) cultured on a mouse astrocyte monolayer on coated thermanox plastic coverslips were examined by transmission electron microscopy (TEM). The cells were fixed in 4% PFA and 2% glutaraldehyde in 0.12M Phosphate Buffer (PB, pH 7.4), and then treated for 45 minutes at RT with 1% OsO_4 (Electron Microscopy Sciences, Hatfield, PA, USA) and 7% glucose in PB, after which they were stained with 1% uranyl acetate (Electron Microscopy Sciences) in maleate buffer (pH 4.5). The cells were then dehydrated in increasing concentrations of ethanol (50°, 70°, 96° and 100°), and washed twice for 10 minutes in 100° ethanol and $CuSO_4$ to complete dehydration. After clearing in propylene oxide (Fluka AG, Buch, Switzerland) and embedding in Durcupan, the Durcupan was polymerized for 24 h at 60 °C. The next day, the coverslips were placed on top of pre-made resin columns and

the resin was polymerized at at 60 ºC for 24 h. Ultrathin sections (75–80 nm) were obtained and then studied under transmissionTEM.

Analysis of human samples

RNA isolation from human post-mortem tissue

Total RNA was isolated from *post-mortem* tissue (10-20 mg) from the substantia nigra and hippocampal cortex of PD patients or healthy subjects. None of these patients carried *GBA1* mutations and in fact, despite contacting many Brain Banks, none could provide us with tissue from *GBA1*-PD patients. The tissue was mechanically disrupted and homogenized 4-5 times with a Potter-Elvehjem tissue homogenizer in buffer RA1 (NucleoSpin® RNA kit) with β-mercaptoethanol. The samples were then passed 6 times through a 0.9 mm syringe needle, and passed through a filter to clear the lysate and reduce viscosity. The extraction protocol for the kit was then followed according to the manufacturer´s instructions, assessing the concentration and quality of the RNA obtained using NanoDrop One.

Summary of the statistical analysis

After first determining whether the data followed a normal distribution using the Shapiro-Wilk test, parametric (unpaired t-test, t-test with Welch correction for different variances, one-way and two-way ANOVA) or non-parametric tests (Mann-Whitney, Kruskal-Wallis tests) were used for the statistical analysis. The ROUT method was applied to score data outliers and $P<0.05$ was considered significant in all the analysis performed to discard the null hypothesis. GraphPad Prism 5.0 and 8.0 was used for all the statistical analyses.

RESULTS

The molecular phenotype of DA neurons derived from PD patients carrying mutations in *GBA1* and healthy controls

As a first approximation, we initially assessed whether general neuronal and midbrain DA markers were expressed by cells during iPSC differentiation. As such, the relative expression of gene transcripts identifying neural progenitors and immature neurons, and those of midbrain DA neurons at specific stages of their differentiation (see below), were measured by RT-qPCR 18 days after commencing the differentiation protocol (Fig. 1). In cultures of control cells and PD cells carrying N370S/wt or L444P/wt *GBA1* mutations, *PAX6* and *TUBB3* expression was detected, as was that of genes encoding transcription factors (*LMX1A*, *LMX1B*, *FOXA2,* and *NURR1*), enzymes (*TH*), monoamine transporters (vesicular monoamine transporter2 -*VMAT2*- and dopamine transporter -*DAT*), as well as the G-protein-coupled inwardly-rectifying potassium channel 2 (*GIRK2)*.[51-61] No significant differences in transcript expression were observed between PD and control cells (Fig. 1A-C), although *TUBB3* and *DAT* expression was significantly weaker in N370S/wt cells than L444P/wt cells (*P<0.05; **P<0.01: Fig. 1C). *GBA1* expression was similar in the three cell types.

After immunostaining cells with antibodies specific to TH, and the general neuronal markers β-III-tubulin (TUJ1) (Supplementary Fig. S1A-J) and MAP2 (Fig. 2A-T), no significant differences were evident between the control (wt/wt)

and PD cultures (N370S/wt or L444P/wt *GBA1*), with 47.1-56.0% TH^+ neurons relative to the $TuJ1^+$ neurons in the cultures at 30-35 DIV (Fig. S1J), or 24.0-28.2% relative to $MAP2^+$ neurons at 50 DIV (Fig. 2J) and 40.4-49.0% at 90 DIV (Fig. 2T). These neurons formed dense networks in all the three conditions (Fig 2A-I, K-S), suggesting a relatively high degree of morphological maturation. TH^+ neurons began expressing the ventral dopaminergic marker FOXA2 early (47-53% $FOXA2^+/TH^+$ neurons at 21 DIV: Fig. 3A-J), like the midbrain DA neuron marker GIRK2 (43.0-47.0% $GIRK2^+/TH^+$ neurons at 54 DIV: Fig. 3K-T), with no significant differences found between the control and PD cultures.

The presence of GABAergic and glutamatergic neurons in the cultures was also analysed, as they are found in the substantia nigra.[61-64] In fact, the proportion TH^+ neurons that were also $GABA^+$ was between 5.7% and 7.3%, with no significant differences between control and PD cultures (Supplementary Fig. S2A-J).

A subpopulation of DA neurons exhibits a glutamatergic phenotype: Effect of N370S and L444P *GBA1* mutations on these neurons

The vesicular glutamate transporter2 (VGLUT2) is expressed by nearly all midbrain DA neurons during embryonic development.[65-68] Although in the adult SN its expression only persists in <20% of these neurons,[61,64,65,69] VGLUT2 may be neuroprotective in PD.[70-74] To determine if a subpopulation of hiPSC-derived DA neurons adopt a glutamatergic phenotype and whether this might be affected by the *GBA1* mutations, cultures were dual immunostained with antibodies against VGLUT2 and TH (Fig. 4A-I). The proportion of TH^+ neurons co-expressing VGLUT2 was 6.6-fold lower in L444P/wt cultures (2.45% ±1.08)

than in wt/wt cultures (16.12% ±6.03, P = 0.012: Fig. 4J). There was also a clear trend towards fewer relative VGLUT2$^+$/TH$^+$ neurons in the N370S/wt cultures than in the wt/wt cells, although this was not statistically significant (P = 0.2: Fig. 4J). Importantly, the percentage of DA neurons co-expressing VGLUT2 in the controls (16.12%) was similar to that *in vivo*.[65] The *SLC17A6/VGLUT2* mRNA expression by cells differentiating for 18 days was then analysed by RT-qPCR, indicating non-significant changes in N370S/wt and in L444P/wt cultures relative to the control cultures (Fig. 4K). However, the effect of each mutation on *VGLUT2* mRNA was reflected by the reduced *VGLUT2* expression in N370S/wt cultures relative to the L444P/wt cultures (**P<0.01: Fig. 4L).

Since VGLUT2 mediates glutamate co-release and storage by DA neurons into synaptic vesicles (SVs),[71] we measured the glutamate in the culture medium. Although the total glutamate concentration was similar in all three conditions (Fig. 4M), when this concentration was expressed relative to the number of VGLUT2$^+$-TH$^+$ neurons (Fig. 4N), there were significant increases (7-23-fold) in the N370S/wt and L444P/wt cultures relative to the control cultures (*P<0.05; ****P<0.0001). Moreover, the glutamate concentration per VGLUT2$^+$-TH$^+$ neuron was significantly higher in L444P/wt than in N370S/wt cultures (****P<0.0001: Fig. 4N). Together, these findings suggest that the lower proportion of TH$^+$ neurons expressing VGLUT2 and the increase in glutamate could enhance neuronal vulnerability in *GBA1*-associated PD.

The impact of *GBA*1 mutations on dopamine release

Dopamine was detected in the cultures under both basal conditions (Fig. 5A) and after KCl-induced depolarization (evoked: Fig. 5B). There was no significant

difference in dopamine content between *GBA1*-PD and control cultures, although there was a trend towards greater evoked release in N370S/wt and L444P/wt cultures. The dopamine released per minute in wt/wt, N370S/wt and L444P/wt cultures was 50, 104 and 146 times greater in evoked than in basal conditions, respectively (Fig. 5C). These increases were significant in N370S/wt (*P<0.05) and L444P/wt cultures (****P<0.001), yet not in the control cultures. Moreover, there was a significant increase in the released dopamine under evoked conditions in the L444P/wt cultures relative to the control cultures (####P<0.0001). Hence, iPSC-derived neurons appear to respond to physiological-like depolarization, and these DA neurons carrying *GBA1* mutations respond more strongly to depolarization than control neurons.

The effect of *GB*A1 mutations on the electrical responses of iPSC-derived DA neurons

It was important to demonstrate that iPSC-derived DA neurons were electrically active and to assess whether the *GBA1* mutations modified the electrophysiological properties of these neurons. Although neurons were active after 80-82 days in culture (data not shown), electrophysiological responses were more consistently found at 90-93 days and thus, the electrical properties of neurons were analysed at this time point. DA neurons were identified by ICC using antibodies against TH and MAP2 after they were recorded, filled with Alexa-Fluor 488 and fixed (Supplementary Fig. S3A-F; see also Supplementary Fig. S5). *GBA1* mutations did not significantly alter the passive properties of DA neurons (Supplementary Fig. S3G-J). In terms of active properties (Supplementary Fig. 4A), a first action potential (AP) was evoked using

depolarizing current pulses in 75% of DA neurons in the wt/wt cultures, as opposed to 100% of N370/wt and L444P/wt DA neurons, although this increase was not significant). Furthermore, more mutant neurons responded with a second AP than wt/wt neurons, although there were no differences between the control and *GBA1* mutant neurons in terms of the threshold, peak amplitude and half amplitude duration of APs (Supplementary Fig. 4B-E). After injecting hyperpolarizing and depolarizing current pulses, the I-V curves had a similar pattern in all three conditions (Supplementary Fig. 4F). Intrinsic repetitive firing of APs was detected, indicating the presence of neurons with the autonomous pacemaking properties typical of substantia nigra DA neurons (Supplementary Fig. 4G).[75-77] However, the effect of *GBA1* mutations on this repetitive firing was not addressed here. Notably, the firing rate of N370S/wt DA neurons was significantly higher than that of the control neurons (*P<0.05; **P<0.01; ***P<0.001: Fig. 6A), meaning that these neurons generated more APs per second for the same injected current. The L444P/wt neurons appeared to have a slightly but not significantly higher firing rate than control neurons. Hence, iPSC-derived DA neurons acquire functional features and N370S/wt DA neurons adopt a hyperexcitable electrical phenotype.

Finally, spontaneous excitatory postsynaptic potential currents (sEPSCs) were analysed in voltage-clamp mode (Fig. 6B), with more mutant neurons developing sEPSCs than control (wt/wt) neurons, although the differences were not significant (Fig. 6C). The amplitude of the sEPSCs was similar in all three conditions (Fig. 6D), yet the frequency of sEPSCs was significantly lower in L444P/wt neurons than in controls (**P<0.01: Fig. 6E).

Our morphological analysis of the recorded TH^+ cells showed that L444P DA neurons had significantly more intersections in the first 60 µm from the cell body than control and N370S/wt neurons (*P<0.05; **P<0.01; ***P<0.001: supplementary Fig. S5A-P). There were no other appreciable changes in morphological parameters (supplementary Fig. S6A-C).

The N370S and L444P *GBA1* mutations alter the ultrastructure of iPSC-derived neurons

We then decided to use TEM to determine whether the presence of *GBA1* mutations alters the ultrastructure of iPSC-neurons cultured for 91-104 days. However, this analysis could not be specifically performed on TH^+ neurons for technical reasons. In contrast to control neurons (Fig. 7A-B), structures resembling degenerative bodies were frequently detected in neurons derived from patients carrying the N370S (Fig. 7C-D) or L444P (Fig. 7E-F) *GBA1* mutations. These structures were full of vacuoles resembling autophagosomes and dysfunctional lysosomes. In fact, autophagosomes, autophagosome-like structures, and autophagosome-like vacuoles, were clearly distinguished in the cell bodies and processes of neurons carrying GBA1 mutations (supplementary Fig. S7B-D), which were barely detected in control neurons (supplementary Fig. S7A). Multilamellar bodies (MLBs) were also abundant in mutant neurons (Fig. 8) and the membrane of the MLB's were more disorganized in N370S (Fig. 8A-C) than in L444P neurons (Fig. 8D-H). Furthermore, the membrane cisternae that integrate the structures shown in Fig. 8F and 8G were perfectly distinguishable as they were cytoplasmic remnants with heterogeneous material enclosed within.

Since mutant GCases are retained in the GA,[4,20,35,40,78] this organelle was also analysed (Fig. 9). In fact, whereas GA dictyosomes had a normal appearance in control iPSC-derived neurons (Fig. 9A), large numbers of abnormal and vacuolated GA dictyosomes were evident in iPSC-derived neurons from patients carrying the N370S (Fig. 9B-C) or L444P mutation (Fig. 9D-F). Indeed, while the percentage of vacuolated dictyosomes in control cells was 10.25%, this number increased to 42.85% and to 82.60% in cells carrying the N370S or the L444P mutation, respectively (Fig. 9G).

In summary, both N370S and L444P *GBA1*-neurons accumulate abundant degenerative bodies, MLBs, vacuolated GA dictyosomes, autophagosomes and dysfunctional lysosomes that could affect neuronal function and vulnerability.

The N370S *GBA1* mutation favours α-synuclein accumulation in DA neurons

α-synuclein is enriched in the presynaptic compartment, and it influences vesicle dynamics, trafficking and neurotransmitter release.[78,79] However, due to its unstable conformation it may undergo misfolding under cellular stress and aggregate in the PD brain, leading to the formation of Lewy bodies, particularly in the substantia nigra.[22,29,78,80] Since a relation between GCase deficits and α-syn aggregation has been reported,[20,27,32,81] we assessed whether α-syn accumulates in the cell body and dendrites of iPSC-derived DA neurons (Fig. 10). Neurons carrying N370S/wt mutation had significantly more aggregates in both cell bodies (**P<0.01: Fig. 10A-M) and dendrites (****P<0.0001: Fig. 10N-Z) relative to wt/wt neurons. However, the number of aggregates in L444P/wt *GBA1* neurons was similar to those in control neurons and significantly lower

than in N370S/wt *GBA1* neurons, both in the soma (***P<0.001: Fig. 10M) and dendrites (****P<0.0001: Fig. 10Z). Furthermore, the N370S/wt *GBA1* culture medium contained more α-syn per TH^+ neuron than that of wt/wt and L444P/wt cultures, although this difference was not significant (Fig. 10Z'). Hence it appears that the two *GBA1* mutations do not have the same effect on the mechanisms driving α-syn aggregation and release by iPSC-derived DA neurons.

Expression of CRYAB in iPSC-derived DA neurons

Small chaperones fulfil several roles, such as acting as molecular sensors of cellular stress or preventing protein misfolding,[82] and mutations in the *GBA1* gene cause alterations in GCase1 folding.[4,32,83] We previously found an upregulation of CRYAB (or HSPB5/alpha-crystallinB) in neural stem cell cultures[84] and hypothesized that this chaperone might be expressed by iPSC-derived DA neurons, especially in those derived from the patients. Immature neurons (30-33 DIV) from wt/wt individuals and from patients carrying the N370S/wt and L444P/wt *GBA1* mutations expressed CRYAB in both their soma and processes (Fig. 11A-I). CRYAB was detected in 25.12% wt/wt TH^+ neurons, whereas nearly twice as many N370S/wt TH^+ neurons expressed CRYAB (47.65% cells; P<0.0001) and 39.19% of the TH^+ L444P/wt cells were $CRYAB^+$ (a non-significant increase of 56% relative to the control neurons: Fig. 11J). As further insight into the molecular mechanism involved, RT-qPCR analysis revealed significantly stronger *CRYAB mRNA* expression in N370S/wt cultures than in wt/wt (**P<0.01: Fig. 11K) or L444P/wt cultures (*P<0.05: Fig. 11L),

indicating that the N370S/wt mutation alters *CRYAB* transcription at early phases of DA neuron differentiation.

Expression of *CRYAB* and *VGLUT2* in the Substantia nigra of PD patients

RNA from the substantia nigra of PD patients (carrying no *GBA1* mutations, as mentioned above) and from healthy control subjects was then obtained, and *CRYAB* mRNA expression was seen to be significantly enhanced in the patients relative to the controls (*P<0.05: Fig. 12A). Similarly, *VGLUT2* mRNA expression was significantly higher in the patient's substantia nigra compared to that of the controls (*P<0.05: Fig. 12A), whereas no differences *DAT*, *TH* or *GBA1* mRNA expression were observed. Furthermore, the expression of the five transcripts studied was similar in the hippocampus of controls and PD patients (Fig. 12B). Therefore, the enhanced *CRYAB* and *VGLUT2* expression in the patient´s substantia nigra supports a role for these molecules in PD etiopathology and/or neuroprotection.

DISCUSSION

The cellular and molecular mechanisms leading to cell dysfunction and neuronal degeneration in *GBA1*-PD are gradually becoming better understood,[6,10,14,35,40,42,85,86] although important issues are still to be resolved. For example, it remains unclear to what extent *GBA1* mutations affect both to mature and developing DA neurons, and also whether N370S and L444P *GBA1* mutations trigger similar or distinct alterations in neurons. Here we show that hiPSC-neurons carrying the N370S or the L444P *GBA1* mutation in heterozygosis show both common (neuron structure, dopamine release) and

distinct (electrical firing rate, α-syn aggregation, VGLUT2 and CRYAB expression) dysfunctional and degenerative features. While both mutations negatively affect neuronal ultrastructure, some features like MLB structure and the number of vacuolated dictyosomes are partially mutation-dependent. Importantly, CRYAB expression is enhanced in N370S immature neurons, as also observed in the SN of PD patients, evidence that CRYAB may possibly serve as an early biomarker and/or molecular target for PD. Furthermore, the enhanced *VGLUT2* expression in the patient´s SN suggests that a glutamatergic phenotype could make DA neurons less vulnerable to neurodegeneration, in line with previous results.[64,72-74] In this context, we report novel findings suggesting that *GBA1* mutations could trigger DA neuron dysfunction and degeneration by dampening *VGLUT2* mRNA and/or protein expression.

VGLUT2 expression in DA neurons is altered by *GBA1* mutations

The yield of DA neurons in our cultures, 40-50% of all neurons were TH^+, is within the ranges reported elsewhere when dual SMAD inhibition-based protocols are employed on hiPSCs in the absence of transcription factor overexpression.[38-40,87-90] However, these proportions are lower than those reported when other protocols are used, some of which include a cell sorting step to enrich DA neuron progenitors.[33,36,45,76,85,91,92] Importantly, nearly 50% of iPSC-derived TH^+ neurons express GIRK2, a marker of DA neurons in the human adult substantia nigra.[52,58] By contrast, only 5-7% of our iPSC-derived DA neurons expressed GABA, a neurotransmitter abundantly expressed by DA neurons in the olfactory bulb and hypothalamus.[59,93,94]

Analysis by RT-qPCR, immunostaining or both indicates that the N370S mutation is associated with significantly weaker *VGLUT2* mRNA expression, whereas there are relatively fewer VGLUT2-TH neurons in L444P cultures. The fact that the two mutations have different effects on *VGLUT2* expression, and on the proportion of DA neurons expressing this glutamate transporter, suggests that they may trigger some distinct actions. These could include direct effects on mRNA transcription, post-translational regulation and/or the activation of protein degradation. To the best of our knowledge this is the first time VGLUT2 has been seen to be potential molecular targets of *GBA1* mutations during the development of mDA neurons from human pluripotent stem cells.

In mice, the large majority of embryonic mDA neurons express VGLUT2.[66-68] Although similar studies have not been performed in human embryos, our data suggest that *GBA1* mutations may affect the glutamatergic and dopaminergic tone of the extracellular milieu of developing DA neurons. Thus, reduced VGLUT2 expression could enhance the vulnerability of DA neurons as VGLUT2 has been reported to be neuroprotective in PD, probably because this transporter promotes glutamate and dopamine storage in SVs.[64,70,71,73,74] Our finding that *VGLUT2 mRNA* is more strongly expressed in the substantia nigra of PD patients than in controls may reflect a role for this transporter in the resilience of the SN to neurodegeneration. However, no direct relationship could be established between VGLUT2 and *GBA1 in vivo* as the post-mortem tissue analysed was from patients who do not carry *GBA1* mutations, as mentioned above.

The N370S and L444P *GBA1* mutations produce a hyperexcitable phenotype in DA neurons

Here we demonstrate that the iPSC-derived DA neurons (from both controls and PD patients) express features of mature and functional neurons, which include the extracellular release of dopamine under KCl stimulation, AP firing, spontaneous activity and intrinsic repetitive firing. However, the fact that dopamine release in response to KCl is stronger in cultures from PD patients than from controls indicates that mutant DA neurons are more sensitive to depolarization. Because VGLUT2 promotes dopamine storage in SVs, stronger release may partially be due to the lower proportion of VGLUT2$^+$/TH$^+$ neurons in mutant *GBA1* cultures. Impaired dopamine release is a feature of PD [95] and our findings suggest that this impairment can be visualized in culture through the increase in dopamine release in response to KCl-mediated depolarization. Because dopamine can be converted into toxic oxidized dopamine,[96,97] the hyper-excitable state of mutant DA neurons that drives stronger dopamine release could have deleterious consequences for these neurons. By contrast, we do not detect reduced basal dopamine levels in our cultures of DA neurons carrying the N370S or L444P GBA1 mutations, consistent with earlier data.[39] However, lower basal dopamine content was reported in iPSC-derived DA neurons from a N370S-*GBA1* individual[33] and in N370S-GBA1 brain organoids.[98] Among the considerations that must be borne in mind when interpreting these results is that the dopamine concentration was expressed as fmol/µl or ng/ml in earlier studies,[33,98] whereas here it was expressed as pg/TH$^+$ neuron because the amount of dopamine released is a function of the number of neurons in the culture. Thus, more studies will be needed to determine the

extent of impaired dopamine release in iPSC-derived DA neurons from PD patients.

The most striking and novel electrophysiological finding of our study is the hyperexcitable phenotype of N370S-*GBA1* neurons compared to control and L444P neurons, with no changes in the activation threshold. This suggests that N370S neurons may have suffered changes in membrane ion channels, although this was not studied here. Multielectrode recording highlighted a deficiency in the spontaneous excitability of immature neurons derived from a PD patient carrying the N370S mutation.[33] However, the firing rate of these N370S neurons increased with time in culture.[33] In midbrain organoids derived from N370S-*GBA1* patients, largely composed of neural progenitors and immature neurons, microelectrode arrays found reduced firing rates at 15 DIV.[98] The different protocols to obtain DA neurons and organoids, and the distinct differentiation/maturation stages at which recordings were made, together with the use of diverse electrophysiological techniques, could partially account for the differences in these results. Here, mature N370S DA neurons (90-93 DIV) were patch-clamp recorded, whereas previous studies were carried out on immature neurons (30 and 52 DIV) derived from a N370S patient,[33] and on N370S organoids (15 DIV) that contain neural progenitors as well as immature neurons, as mentioned above.[98]

Higher firing frequencies have been reported in DA neurons from the substantia nigra *in vivo* after proteasome inhibition.[99] Since α-syn aggregates can affect the ubiquitin-proteasome system,[37,78,79,100,101] α-syn accumulation in N370S-neurons could be involved in promoting hyperexcitability. In this sense, increased firing frequencies in *DNAJC6* mutant midbrain-like organoids, a

model of early-onset PD, coincide with α-syn aggregation.[102] Here, electrical hyperexcitability was only evident in N370S-*GBA1* neurons, suggesting a correlation between increased α-syn aggregation and altered electrical firing, as reported in other neuronal systems.[79,103,104] By contrast, dopamine release from both N370S and L444P mutant neurons is altered in response to KCl-induced depolarization, both in the presence (N370S) and absence (L444P neurons) of significant α-syn aggregation.

The N370S and L444P *GBA1* mutations disrupt neuronal ultrastructure, but they produce different effects on α-synuclein and CRYAB

Our EM study shows that neurons carrying GBA1 mutations develop clear signs of degeneration, accumulating degenerative bodies, MLBs and vacuolated Golgi dictyosomes, with these features being partially mutation-specific. Although some of these features were previously observed in N370S fibroblasts, such as MLBs,[28,35] this is the first time they are reported in human neurons derived from *GBA1*-PD patients. Therefore, our culture system allows clear features of neurodegeneration to be detected in iPSC-derived neurons, in contrast to the idea that this process is little evident in these human neurons.

Moreover, the accumulation of α-syn aggregates in dendrites and cell bodies of TH^+/$MAP2^+$ neurons carrying the N370S/wt *GBA1* mutation supports the feasibility of using this cell model to study neurodegeneration in PD. This accumulation is consistent with a previous study where such aggregates were also detected by ICC,[33] although ultrastructural alterations were not reported. Nevertheless, increased α-syn release and an enlarged lysosomal compartment in N370S neurons have been reported previously.[40] L444P neurons did not

accumulate significant α-syn or release this protein, suggesting that the ultrastructural defects in these neurons occur in the absence of α-syn aggregates, or alternatively, that the aberrant α-syn structures that might have formed in L444P neurons are rapidly degraded. By contrast, α-syn accumulation was previously detected in Western blots of L444P cell extracts[39] and the overexpression of this mutation in neurons was sufficient to induce lysosomal dysfunction.[78,85] The α-syn accumulation in *GBA1*-mutant neurons could be a consequence of impaired CMA, which is more deficient in iPSC-derived DA neurons carrying N370S than L444P mutations.[32,101] Together, our results suggest that the aggregation and the degradation of aberrant proteins could be affected distinctly by the two *GBA1* mutations in the context of PD.

Notably, we found a higher proportion of DA neurons expressing CRYAB and *CRYAB* mRNA upregulation in cultures from N370S PD patients. Similarly, CRYAB upregulation was described in the substantia nigra of PD patients, particularly in cytoplasmic inclusions of some glial cells.[105]. This protein may protect against the aggregation, and toxicity of amyloidogenic proteins, and it has been shown to participate in the inhibition of α-syn accumulation.[106-109] Indeed, the upregulation of *CRYAB* mRNA in the substantia nigra but not the hippocampal cortex of PD patients suggests CRYAB could be specifically involved in PD. However, CRYAB has not been previously described as an ER-associated and/or UPR-associated chaperone in cellular models of neurodegeneration.[40,78,101] Furthermore, the higher abundance of *CRYAB* mRNA and of $CRYAB^+/TH^+$ neurons at early stages of iPSC differentiation, well before α-syn aggregation in N370S neurons, suggest that CRYAB upregulation may act as a stress sensor in early stages of the neurodegenerative process.

In conclusion, our study uncovers common and distinct effects of the N370S and L444P *GBA1* mutations in multiple processes in neurons, for the first time identifying VGLUT2 and CRYAB as potential molecular targets and/or biomarkers of early stages of *GBA1*-associated PD.

ACKNOWLEDGEMENTS

We thank the following individuals from the Instituto Cajal-CSIC (Madrid, Spain): Dr Eva Díaz-Guerra and Dr Alicia Hernández-Vivanco for their help with the experiments; Paula Vicario del Río, Silvia Calero, Pablo Fernández, and Lucía Vicario del Río for their help with the image analysis and formatting the reference list; and Mª José Román for her technical support. We also thank Dr Mark Sefton (BiomedRed SL, Madrid, Spain) for English editing advice and the "Unidad de Imagen Científica y Microscopía" (Instituto Cajal-CSIC) for helping us with the analysis of α-syn aggregates. We appreciate the contribution of the responsible and coordinator personnel of the CIEN tissue bank (BT-CIEN, Fundación CIEN, Madrid, Spain) and CeGeN-ISCIII (Santiago de Compostela, Spain) for providing us with post-mortem tissue and performing the genotype analysis, respectively.

FUNDING

This work was funded by grants from the Spanish MINECO and MICIN/AEI: SAF2016-80419-R, PID2019-109059RB-I00, PID2022-137076OB-I00 to C.V. and PID2022-143181OB100 to R.M.; from ISCIII: CIBERNED CB06/05/065 to C.V. and CB06/05/0055 to R.M.; from the Fundación Ramón Areces: CIVP18A3941 to C.V. and R.M.; and from the Michael J. Fox Foundation for

Parkinson's Research to R.M. E.R.T received a FPI fellowship from the MINECO.

The study was approved by the Commission of Guarantees for the Donation and Utilization of Human Cells and Tissues, Instituto de Salud Carlos III (ISCIII), Spain (approval numbers: 3212701, 4083311, 4103331 and 5224261). Informed consent was obtained from all the patients.

DATA AVAILABILITY STATEMENT

The data that support the findings of this study are available on reasonable request from the corresponding author.

COMPETING INTERESTS

The authors have no conflict of interest.

REFERENCES

1. Sidransky E, Nalls MA, Aasly JO*, et al*. Multicenter analysis of glucocerebrosidase mutations in Parkinson's disease. *N Engl J Med*. Oct 22 2009;361(17):1651-61. doi:10.1056/NEJMoa0901281
2. Gegg ME, Menozzi E, Schapira AHV. Glucocerebrosidase-associated Parkinson disease: Pathogenic mechanisms and potential drug treatments. *Neurobiol Dis*. May 2022;166:105663. doi:10.1016/j.nbd.2022.105663
3. Cilia R, Tunesi S, Marotta G*, et al*. Survival and dementia in GBA-associated Parkinson's disease: The mutation matters. *Ann Neurol*. Nov 2016;80(5):662-673. doi:10.1002/ana.24777
4. Sidransky E, Lopez G. The link between the GBA gene and parkinsonism. *Lancet Neurol*. Nov 2012;11(11):986-98. doi:10.1016/S1474-4422(12)70190-4
5. Blandini F, Cilia R, Cerri S*, et al*. Glucocerebrosidase mutations and synucleinopathies: Toward a model of precision medicine. *Mov Disord*. Jan 2019;34(1):9-21. doi:10.1002/mds.27583
6. Baden P, Yu C, Deleidi M. Insights into GBA Parkinson's disease pathology and therapy with induced pluripotent stem cell model systems. *Neurobiol Dis*. Jul 2019;127:1-12. doi:10.1016/j.nbd.2019.01.023
7. Poewe W, Seppi K, Marini K, Mahlknecht P. New hopes for disease modification in Parkinson's Disease. *Neuropharmacology*. Jul 2020;171:108085. doi:10.1016/j.neuropharm.2020.108085
8. Bloem BR, Okun MS, Klein C. Parkinson's disease. *Lancet*. Jun 12 2021;397(10291):2284-2303. doi:10.1016/S0140-6736(21)00218-X
9. Cavallieri F, Cury RG, Guimaraes T*, et al*. Recent Advances in the Treatment of Genetic Forms of Parkinson's Disease: Hype or Hope? *Cells*. Feb 27 2023;12(5)doi:10.3390/cells12050764
10. Chatterjee D, Krainc D. Mechanisms of Glucocerebrosidase Dysfunction in Parkinson's Disease. *J Mol Biol*. Jun 15 2023;435(12):168023. doi:10.1016/j.jmb.2023.168023
11. Seto-Salvia N, Pagonabarraga J, Houlden H*, et al*. Glucocerebrosidase mutations confer a greater risk of dementia during Parkinson's disease course. *Mov Disord*. Mar 2012;27(3):393-9. doi:10.1002/mds.24045
12. Rodriguez-Traver E, Diaz-Guerra E, Rodriguez C*, et al*. A collection of integration-free iPSCs derived from Parkinson's disease patients carrying mutations in the GBA1 gene. *Stem Cell Res*. Jul 2019;38:101482. doi:10.1016/j.scr.2019.101482
13. Rodriguez-Traver E, Rodriguez C, Diaz-Guerra E*, et al*. Generation of an integration-free iPSC line, ICCSICi005-A, derived from a Parkinson's disease patient carrying the L444P mutation in the GBA1 gene. *Stem Cell Res*. Oct 2019;40:101578. doi:10.1016/j.scr.2019.101578
14. Garcia-Sanz P, J MFGA, Moratalla R. The Role of Cholesterol in alpha-Synuclein and Lewy Body Pathology in GBA1 Parkinson's Disease. *Mov Disord*. May 2021;36(5):1070-1085. doi:10.1002/mds.28396
15. Schapira AHV, Chaudhuri KR, Jenner P. Non-motor features of Parkinson disease. *Nat Rev Neurosci*. Aug 2017;18(8):509. doi:10.1038/nrn.2017.91
16. Mata IF, Leverenz JB, Weintraub D*, et al*. GBA Variants are associated with a distinct pattern of cognitive deficits in Parkinson's disease. *Mov Disord*. Jan 2016;31(1):95-102. doi:10.1002/mds.26359
17. Jiang Z, Huang Y, Zhang P*, et al*. Characterization of a pathogenic variant in GBA for Parkinson's disease with mild cognitive impairment patients. *Mol Brain*. Jul 8 2020;13(1):102. doi:10.1186/s13041-020-00637-x
18. Obeso JA, Monje MHG, Matarazzo M. Major advances in Parkinson's disease over the past two decades and future research directions. *Lancet Neurol*. Dec 2022;21(12):1076-1079. doi:10.1016/S1474-4422(22)00448-3

19. Shults CW. Lewy bodies. *Proc Natl Acad Sci U S A*. Feb 7 2006;103(6):1661-8. doi:10.1073/pnas.0509567103
20. Mazzulli JR, Xu YH, Sun Y*, et al*. Gaucher disease glucocerebrosidase and alpha-synuclein form a bidirectional pathogenic loop in synucleinopathies. *Cell*. Jul 8 2011;146(1):37-52. doi:10.1016/j.cell.2011.06.001
21. Surmeier DJ, Obeso JA, Halliday GM. Selective neuronal vulnerability in Parkinson disease. *Nat Rev Neurosci*. Jan 20 2017;18(2):101-113. doi:10.1038/nrn.2016.178
22. Shahmoradian SH, Lewis AJ, Genoud C*, et al*. Lewy pathology in Parkinson's disease consists of crowded organelles and lipid membranes. *Nat Neurosci*. Jul 2019;22(7):1099-1109. doi:10.1038/s41593-019-0423-2
23. Fares MB, Jagannath S, Lashuel HA. Reverse engineering Lewy bodies: how far have we come and how far can we go? *Nat Rev Neurosci*. Feb 2021;22(2):111-131. doi:10.1038/s41583-020-00416-6
24. Gegg ME, Sweet L, Wang BH, Shihabuddin LS, Sardi SP, Schapira AH. No evidence for substrate accumulation in Parkinson brains with GBA mutations. *Mov Disord*. Jul 2015;30(8):1085-9. doi:10.1002/mds.26278
25. Rocha EM, Smith GA, Park E*, et al*. Progressive decline of glucocerebrosidase in aging and Parkinson's disease. *Ann Clin Transl Neurol*. Apr 2015;2(4):433-8. doi:10.1002/acn3.177
26. Yap TL, Gruschus JM, Velayati A*, et al*. Alpha-synuclein interacts with Glucocerebrosidase providing a molecular link between Parkinson and Gaucher diseases. *J Biol Chem*. Aug 12 2011;286(32):28080-8. doi:10.1074/jbc.M111.237859
27. Zunke F, Moise AC, Belur NR*, et al*. Reversible Conformational Conversion of alpha-Synuclein into Toxic Assemblies by Glucosylceramide. *Neuron*. Jan 3 2018;97(1):92-107 e10. doi:10.1016/j.neuron.2017.12.012
28. Garcia-Sanz P, Orgaz L, Bueno-Gil G*, et al*. N370S-GBA1 mutation causes lysosomal cholesterol accumulation in Parkinson's disease. *Mov Disord*. Oct 2017;32(10):1409-1422. doi:10.1002/mds.27119
29. Goker-Alpan O, Stubblefield BK, Giasson BI, Sidransky E. Glucocerebrosidase is present in alpha-synuclein inclusions in Lewy body disorders. *Acta Neuropathol*. Nov 2010;120(5):641-9. doi:10.1007/s00401-010-0741-7
30. Henderson MX, Sedor S, McGeary I*, et al*. Glucocerebrosidase Activity Modulates Neuronal Susceptibility to Pathological alpha-Synuclein Insult. *Neuron*. Mar 4 2020;105(5):822-836 e7. doi:10.1016/j.neuron.2019.12.004
31. Horowitz M, Braunstein H, Zimran A, Revel-Vilk S, Goker-Alpan O. Lysosomal functions and dysfunctions: Molecular and cellular mechanisms underlying Gaucher disease and its association with Parkinson disease. *Adv Drug Deliv Rev*. Aug 2022;187:114402. doi:10.1016/j.addr.2022.114402
32. Kuo SH, Tasset I, Cheng MM*, et al*. Mutant glucocerebrosidase impairs alpha-synuclein degradation by blockade of chaperone-mediated autophagy. *Sci Adv*. Feb 11 2022;8(6):eabm6393. doi:10.1126/sciadv.abm6393
33. Woodard CM, Campos BA, Kuo SH*, et al*. iPSC-derived dopamine neurons reveal differences between monozygotic twins discordant for Parkinson's disease. *Cell Rep*. Nov 20 2014;9(4):1173-82. doi:10.1016/j.celrep.2014.10.023
34. Burbulla LF, Song P, Mazzulli JR*, et al*. Dopamine oxidation mediates mitochondrial and lysosomal dysfunction in Parkinson's disease. *Science*. Sep 22 2017;357(6357):1255-1261. doi:10.1126/science.aam9080
35. Garcia-Sanz P, Orgaz L, Fuentes JM, Vicario C, Moratalla R. Cholesterol and multilamellar bodies: Lysosomal dysfunction in GBA-Parkinson disease. *Autophagy*. 2018;14(4):717-718. doi:10.1080/15548627.2018.1427396
36. Lang C, Campbell KR, Ryan BJ*, et al*. Single-Cell Sequencing of iPSC-Dopamine Neurons Reconstructs Disease Progression and Identifies HDAC4 as a Regulator of Parkinson Cell Phenotypes. *Cell Stem Cell*. Jan 3 2019;24(1):93-106 e6. doi:10.1016/j.stem.2018.10.023

37. Stojkovska I, Wani WY, Zunke F*, et al*. Rescue of alpha-synuclein aggregation in Parkinson's patient neurons by synergistic enhancement of ER proteostasis and protein trafficking. *Neuron*. Nov 9 2021;doi:10.1016/j.neuron.2021.10.032
38. Schondorf DC, Ivanyuk D, Baden P*, et al*. The NAD+ Precursor Nicotinamide Riboside Rescues Mitochondrial Defects and Neuronal Loss in iPSC and Fly Models of Parkinson's Disease. *Cell Rep*. Jun 5 2018;23(10):2976-2988. doi:10.1016/j.celrep.2018.05.009
39. Schondorf DC, Aureli M, McAllister FE*, et al*. iPSC-derived neurons from GBA1-associated Parkinson's disease patients show autophagic defects and impaired calcium homeostasis. *Nat Commun*. Jun 6 2014;5:4028. doi:10.1038/ncomms5028
40. Fernandes HJ, Hartfield EM, Christian HC*, et al*. ER Stress and Autophagic Perturbations Lead to Elevated Extracellular alpha-Synuclein in GBA-N370S Parkinson's iPSC-Derived Dopamine Neurons. *Stem Cell Reports*. Mar 8 2016;6(3):342-56. doi:10.1016/j.stemcr.2016.01.013
41. Beccano-Kelly DA, Cherubini M, Mousba Y*, et al*. Calcium dysregulation combined with mitochondrial failure and electrophysiological maturity converge in Parkinson's iPSC-dopamine neurons. *iScience*. Jul 21 2023;26(7):107044. doi:10.1016/j.isci.2023.107044
42. Pradas E, Martinez-Vicente M. The Consequences of GBA Deficiency in the Autophagy-Lysosome System in Parkinson's Disease Associated with GBA. *Cells*. Jan 3 2023;12(1)doi:10.3390/cells12010191
43. Rodriguez-Traver E, Diaz-Guerra E, Rodriguez C*, et al*. A collection of three integration-free iPSCs derived from old male and female healthy subjects. *Stem Cell Res*. Jan 2020;42:101663. doi:10.1016/j.scr.2019.101663
44. Kriks S, Shim JW, Piao J*, et al*. Dopamine neurons derived from human ES cells efficiently engraft in animal models of Parkinson's disease. *Nature*. Nov 6 2011;480(7378):547-51. doi:10.1038/nature10648
45. Doi D, Samata B, Katsukawa M*, et al*. Isolation of human induced pluripotent stem cell-derived dopaminergic progenitors by cell sorting for successful transplantation. *Stem Cell Reports*. Mar 11 2014;2(3):337-50. doi:10.1016/j.stemcr.2014.01.013
46. Kirkeby A, Grealish S, Wolf DA*, et al*. Generation of regionally specified neural progenitors and functional neurons from human embryonic stem cells under defined conditions. *Cell Rep*. Jun 28 2012;1(6):703-14. doi:10.1016/j.celrep.2012.04.009
47. Nieto-Estevez V, Oueslati-Morales CO, Li L, Pickel J, Morales AV, Vicario-Abejon C. Brain Insulin-Like Growth Factor-I Directs the Transition from Stem Cells to Mature Neurons During Postnatal/Adult Hippocampal Neurogenesis. *Stem Cells*. Aug 2016;34(8):2194-209. doi:10.1002/stem.2397
48. Schmittgen TD, Livak KJ. Analyzing real-time PCR data by the comparative C(T) method. *Nat Protoc*. 2008;3(6):1101-8. doi:10.1038/nprot.2008.73
49. Pfaffl MW. A new mathematical model for relative quantification in real-time RT-PCR. *Nucleic Acids Res*. May 1 2001;29(9):e45. doi:10.1093/nar/29.9.e45
50. Kutzing MK, Langhammer CG, Luo V, Lakdawala H, Firestein BL. Automated Sholl analysis of digitized neuronal morphology at multiple scales. *J Vis Exp*. Nov 14 2010;(45)doi:10.3791/2354
51. Chu Y, Kompoliti K, Cochran EJ, Mufson EJ, Kordower JH. Age-related decreases in Nurr1 immunoreactivity in the human substantia nigra. *J Comp Neurol*. Aug 26 2002;450(3):203-14. doi:10.1002/cne.10261
52. Mendez I, Sanchez-Pernaute R, Cooper O*, et al*. Cell type analysis of functional fetal dopamine cell suspension transplants in the striatum and substantia nigra of patients with Parkinson's disease. *Brain*. Jul 2005;128(Pt 7):1498-510. doi:10.1093/brain/awh510
53. Andersson E, Tryggvason U, Deng Q*, et al*. Identification of intrinsic determinants of midbrain dopamine neurons. *Cell*. Jan 27 2006;124(2):393-405. doi:10.1016/j.cell.2005.10.037

54. Kittappa R, Chang WW, Awatramani RB, McKay RD. The foxa2 gene controls the birth and spontaneous degeneration of dopamine neurons in old age. *PLoS Biol*. Dec 2007;5(12):e325. doi:10.1371/journal.pbio.0050325
55. Friling S, Andersson E, Thompson LH*, et al*. Efficient production of mesencephalic dopamine neurons by Lmx1a expression in embryonic stem cells. *Proc Natl Acad Sci U S A*. May 5 2009;106(18):7613-8. doi:10.1073/pnas.0902396106
56. Lee HS, Bae EJ, Yi SH*, et al*. Foxa2 and Nurr1 synergistically yield A9 nigral dopamine neurons exhibiting improved differentiation, function, and cell survival. *Stem Cells*. Mar 31 2010;28(3):501-12. doi:10.1002/stem.294
57. Sanchez-Danes A, Richaud-Patin Y, Carballo-Carbajal I*, et al*. Disease-specific phenotypes in dopamine neurons from human iPS-based models of genetic and sporadic Parkinson's disease. *EMBO Mol Med*. May 2012;4(5):380-95. doi:10.1002/emmm.201200215
58. Reyes S, Fu Y, Double K*, et al*. GIRK2 expression in dopamine neurons of the substantia nigra and ventral tegmental area. *J Comp Neurol*. Aug 15 2012;520(12):2591-607. doi:10.1002/cne.23051
59. Rodriguez-Traver E, Solis O, Diaz-Guerra E*, et al*. Role of Nurr1 and GDNF in the Generation and Differentiation of Dopaminergic Neurons from Stem Cells. *Neurotox Res*. Jul 2016;30(1):14-31. doi:10.1007/s12640-015-9586-0
60. Kamath T, Abdulraouf A, Burris SJ*, et al*. Single-cell genomic profiling of human dopamine neurons identifies a population that selectively degenerates in Parkinson's disease. *Nat Neurosci*. May 2022;25(5):588-595. doi:10.1038/s41593-022-01061-1
61. Garritsen O, van Battum EY, Grossouw LM, Pasterkamp RJ. Development, wiring and function of dopamine neuron subtypes. *Nat Rev Neurosci*. Mar 2023;24(3):134-152. doi:10.1038/s41583-022-00669-3
62. Rodriguez M, Gonzalez-Hernandez T. Electrophysiological and morphological evidence for a GABAergic nigrostriatal pathway. *J Neurosci*. Jun 1 1999;19(11):4682-94. doi:10.1523/JNEUROSCI.19-11-04682.1999
63. Tritsch NX, Ding JB, Sabatini BL. Dopaminergic neurons inhibit striatal output through non-canonical release of GABA. *Nature*. Oct 11 2012;490(7419):262-6. doi:10.1038/nature11466
64. Trudeau LE, Hnasko TS, Wallen-Mackenzie A, Morales M, Rayport S, Sulzer D. The multilingual nature of dopamine neurons. *Prog Brain Res*. 2014;211:141-64. doi:10.1016/B978-0-444-63425-2.00006-4
65. Steinkellner T, Zell V, Farino ZJ*, et al*. Role for VGLUT2 in selective vulnerability of midbrain dopamine neurons. *J Clin Invest*. Feb 1 2018;128(2):774-788. doi:10.1172/JCI95795
66. Dumas S, Wallen-Mackenzie A. Developmental Co-expression of Vglut2 and Nurr1 in a Mes-Di-Encephalic Continuum Preceeds Dopamine and Glutamate Neuron Specification. *Front Cell Dev Biol*. 2019;7:307. doi:10.3389/fcell.2019.00307
67. Kouwenhoven WM, Fortin G, Penttinen AM*, et al*. VGluT2 Expression in Dopamine Neurons Contributes to Postlesional Striatal Reinnervation. *J Neurosci*. Oct 21 2020;40(43):8262-8275. doi:10.1523/JNEUROSCI.0823-20.2020
68. Eskenazi D, Malave L, Mingote S*, et al*. Dopamine Neurons That Cotransmit Glutamate, From Synapses to Circuits to Behavior. *Front Neural Circuits*. 2021;15:665386. doi:10.3389/fncir.2021.665386
69. Pereira Luppi M, Azcorra M, Caronia-Brown G*, et al*. Sox6 expression distinguishes dorsally and ventrally biased dopamine neurons in the substantia nigra with distinctive properties and embryonic origins. *Cell Rep*. Nov 9 2021;37(6):109975. doi:10.1016/j.celrep.2021.109975
70. Kashani A, Betancur C, Giros B, Hirsch E, El Mestikawy S. Altered expression of vesicular glutamate transporters VGLUT1 and VGLUT2 in Parkinson disease. *Neurobiol Aging*. Apr 2007;28(4):568-78. doi:10.1016/j.neurobiolaging.2006.02.010

71. Hnasko TS, Chuhma N, Zhang H, *et al*. Vesicular glutamate transport promotes dopamine storage and glutamate corelease in vivo. *Neuron*. Mar 11 2010;65(5):643-56. doi:10.1016/j.neuron.2010.02.012
72. Shen H, Marino RAM, McDevitt RA, *et al*. Genetic deletion of vesicular glutamate transporter in dopamine neurons increases vulnerability to MPTP-induced neurotoxicity in mice. *Proc Natl Acad Sci U S A*. Dec 4 2018;115(49):E11532-E11541. doi:10.1073/pnas.1800886115
73. Buck SA, Erickson-Oberg MQ, Bhatte SH, *et al*. Roles of VGLUT2 and Dopamine/Glutamate Co-Transmission in Selective Vulnerability to Dopamine Neurodegeneration. *ACS Chem Neurosci*. Jan 19 2022;13(2):187-193. doi:10.1021/acschemneuro.1c00741
74. Steinkellner T, Conrad WS, Kovacs I, *et al*. Dopamine neurons exhibit emergent glutamatergic identity in Parkinson's disease. *Brain*. Nov 19 2021;doi:10.1093/brain/awab373
75. Guzman JN, Sanchez-Padilla J, Chan CS, Surmeier DJ. Robust pacemaking in substantia nigra dopaminergic neurons. *J Neurosci*. Sep 2 2009;29(35):11011-9. doi:10.1523/JNEUROSCI.2519-09.2009
76. Li H, Jiang H, Li H, Li L, Yan Z, Feng J. Generation of human A9 dopaminergic pacemakers from induced pluripotent stem cells. *Mol Psychiatry*. Nov 2022;27(11):4407-4418. doi:10.1038/s41380-022-01628-1
77. Pu J, Lin L, Jiang H, *et al*. Parkin Maintains Robust Pacemaking in Human Induced Pluripotent Stem Cell-Derived A9 Dopaminergic Neurons. *Mov Disord*. Jul 2023;38(7):1273-1281. doi:10.1002/mds.29434
78. Zalon AJ, Quiriconi DJ, Pitcairn C, Mazzulli JR. alpha-Synuclein: Multiple pathogenic roles in trafficking and proteostasis pathways in Parkinson's disease. *Neuroscientist*. Feb 29 2024:10738584241232963. doi:10.1177/10738584241232963
79. Calabresi P, Di Lazzaro G, Marino G, Campanelli F, Ghiglieri V. Advances in understanding the function of alpha-synuclein: implications for Parkinson's disease. *Brain*. Sep 1 2023;146(9):3587-3597. doi:10.1093/brain/awad150
80. Alam P, Bousset L, Melki R, Otzen DE. alpha-synuclein oligomers and fibrils: a spectrum of species, a spectrum of toxicities. *J Neurochem*. Sep 2019;150(5):522-534. doi:10.1111/jnc.14808
81. Vieira SRL, Schapira AHV. Glucocerebrosidase mutations and Parkinson disease. *J Neural Transm (Vienna)*. Sep 2022;129(9):1105-1117. doi:10.1007/s00702-022-02531-3
82. Hayashi J, Carver JA. The multifaceted nature of alphaB-crystallin. *Cell Stress Chaperones*. Jul 2020;25(4):639-654. doi:10.1007/s12192-020-01098-w
83. Patnaik S, Zheng W, Choi JH, *et al*. Discovery, structure-activity relationship, and biological evaluation of noninhibitory small molecule chaperones of glucocerebrosidase. *J Med Chem*. Jun 28 2012;55(12):5734-48. doi:10.1021/jm300063b
84. Nieto-Estevez V, Pignatelli J, Arauzo-Bravo MJ, Hurtado-Chong A, Vicario-Abejon C. A global transcriptome analysis reveals molecular hallmarks of neural stem cell death, survival, and differentiation in response to partial FGF-2 and EGF deprivation. *PLoS One*. 2013;8(1):e53594. doi:10.1371/journal.pone.0053594
85. Mazzulli JR, Zunke F, Isacson O, Studer L, Krainc D. alpha-Synuclein-induced lysosomal dysfunction occurs through disruptions in protein trafficking in human midbrain synucleinopathy models. *Proc Natl Acad Sci U S A*. Feb 16 2016;113(7):1931-6. doi:10.1073/pnas.1520335113
86. Brooker SM, Naylor GE, Krainc D. Cell biology of Parkinson's disease: Mechanisms of synaptic, lysosomal, and mitochondrial dysfunction. *Curr Opin Neurobiol*. Apr 2024;85:102841. doi:10.1016/j.conb.2024.102841
87. Rhee YH, Ko JY, Chang MY, *et al*. Protein-based human iPS cells efficiently generate functional dopamine neurons and can treat a rat model of Parkinson disease. *J Clin Invest*. Jun 2011;121(6):2326-35. doi:10.1172/JCI45794

88. Hartfield EM, Yamasaki-Mann M, Ribeiro Fernandes HJ, *et al*. Physiological characterisation of human iPS-derived dopaminergic neurons. *PLoS One*. 2014;9(2):e87388. doi:10.1371/journal.pone.0087388
89. Schweitzer JS, Song B, Herrington TM, *et al*. Personalized iPSC-Derived Dopamine Progenitor Cells for Parkinson's Disease. *N Engl J Med*. May 14 2020;382(20):1926-1932. doi:10.1056/NEJMoa1915872
90. Laperle AH, Sances S, Yucer N, *et al*. iPSC modeling of young-onset Parkinson's disease reveals a molecular signature of disease and novel therapeutic candidates. *Nat Med*. Feb 2020;26(2):289-299. doi:10.1038/s41591-019-0739-1
91. Chung CY, Khurana V, Auluck PK, *et al*. Identification and rescue of alpha-synuclein toxicity in Parkinson patient-derived neurons. *Science*. Nov 22 2013;342(6161):983-7. doi:10.1126/science.1245296
92. Kishinevsky S, Wang T, Rodina A, *et al*. HSP90-incorporating chaperome networks as biosensor for disease-related pathways in patient-specific midbrain dopamine neurons. *Nat Commun*. Oct 19 2018;9(1):4345. doi:10.1038/s41467-018-06486-6
93. Bjorklund A, Dunnett SB. Dopamine neuron systems in the brain: an update. *Trends Neurosci*. May 2007;30(5):194-202. doi:10.1016/j.tins.2007.03.006
94. Nieto-Estevez V, Defterali C, Vicario C. Distinct Effects of BDNF and NT-3 on the Dendrites and Presynaptic Boutons of Developing Olfactory Bulb GABAergic Interneurons In Vitro. *Cell Mol Neurobiol*. Jul 2022;42(5):1399-1417. doi:10.1007/s10571-020-01030-x
95. Cramb KML, Beccano-Kelly D, Cragg SJ, Wade-Martins R. Impaired dopamine release in Parkinson's disease. *Brain*. Aug 1 2023;146(8):3117-3132. doi:10.1093/brain/awad064
96. Zhang S, Wang R, Wang G. Impact of Dopamine Oxidation on Dopaminergic Neurodegeneration. *ACS Chem Neurosci*. Feb 20 2019;10(2):945-953. doi:10.1021/acschemneuro.8b00454
97. Song P, Peng W, Sauve V, *et al*. Parkinson's disease-linked parkin mutation disrupts recycling of synaptic vesicles in human dopaminergic neurons. *Neuron*. Dec 6 2023;111(23):3775-3788 e7. doi:10.1016/j.neuron.2023.08.018
98. Rosety I, Zagare A, Saraiva C, *et al*. Impaired neuron differentiation in GBA-associated Parkinson's disease is linked to cell cycle defects in organoids. *NPJ Parkinsons Dis*. Dec 18 2023;9(1):166. doi:10.1038/s41531-023-00616-8
99. Subramaniam M, Kern B, Vogel S, Klose V, Schneider G, Roeper J. Selective increase of in vivo firing frequencies in DA SN neurons after proteasome inhibition in the ventral midbrain. *Eur J Neurosci*. Sep 2014;40(6):2898-909. doi:10.1111/ejn.12660
100. Lindersson E, Beedholm R, Hojrup P, *et al*. Proteasomal inhibition by alpha-synuclein filaments and oligomers. *J Biol Chem*. Mar 26 2004;279(13):12924-34. doi:10.1074/jbc.M306390200
101. Onal G, Yalcin-Cakmakli G, Ozcelik CE, *et al*. Variant-specific effects of GBA1 mutations on dopaminergic neuron proteostasis. *J Neurochem*. Apr 20 2024;doi:10.1111/jnc.16114
102. Wulansari N, Darsono WHW, Woo HJ, *et al*. Neurodevelopmental defects and neurodegenerative phenotypes in human brain organoids carrying Parkinson's disease-linked DNAJC6 mutations. *Sci Adv*. Feb 2021;7(8)doi:10.1126/sciadv.abb1540
103. Tozzi A, Sciaccaluga M, Loffredo V, *et al*. Dopamine-dependent early synaptic and motor dysfunctions induced by alpha-synuclein in the nigrostriatal circuit. *Brain*. Dec 16 2021;144(11):3477-3491. doi:10.1093/brain/awab242
104. Tomagra G, Franchino C, Cesano F, *et al*. Alpha-synuclein oligomers alter the spontaneous firing discharge of cultured midbrain neurons. *Front Cell Neurosci*. 2023;17:1078550. doi:10.3389/fncel.2023.1078550
105. Liu Y, Zhou Q, Tang M, *et al*. Upregulation of alphaB-crystallin expression in the substantia nigra of patients with Parkinson's disease. *Neurobiol Aging*. Apr 2015;36(4):1686-1691. doi:10.1016/j.neurobiolaging.2015.01.015

106. Masilamoni JG, Jesudason EP, Baben B, Jebaraj CE, Dhandayuthapani S, Jayakumar R. Molecular chaperone alpha-crystallin prevents detrimental effects of neuroinflammation. *Biochim Biophys Acta*. Mar 2006;1762(3):284-93. doi:10.1016/j.bbadis.2005.11.007
107. Bruinsma IB, Bruggink KA, Kinast K*, et al*. Inhibition of alpha-synuclein aggregation by small heat shock proteins. *Proteins*. Oct 2011;79(10):2956-67. doi:10.1002/prot.23152
108. Cox D, Carver JA, Ecroyd H. Preventing alpha-synuclein aggregation: the role of the small heat-shock molecular chaperone proteins. *Biochim Biophys Acta*. Sep 2014;1842(9):1830-43. doi:10.1016/j.bbadis.2014.06.024
109. Scheidt T, Carozza JA, Kolbe CC*, et al*. The binding of the small heat-shock protein alphaB-crystallin to fibrils of alpha-synuclein is driven by entropic forces. *Proc Natl Acad Sci U S A*. Sep 21 2021;118(38)doi:10.1073/pnas.2108790118

FIGURE LEGENDS

Figure 1 Gene expression in differentiating cultures of iPSCs derived from PD patients carrying the N370S or the L444P *GBA1* mutation and healthy subjects. (A-C) Total RNA was extracted from the cells after 18 days of differentiation, reverse transcribed to cDNA and analysed by RT-qPCR using the oligonucleotide primers listed in Supplementary Table 1. Transcript expression was largely similar in the three conditions, although a significantly lower expression of *TUBB3* and *DAT* was found in N370S/wt relative to the L444P/wt cultures (*P<0.05; **P<0.01: C). Statistical analysis was carried out using an unpaired Student's t test to compare the mean (±SEM) values of n = 6-9 cultures per genotype from 3 experiments performed in triplicate.

Figure 2 The N370S and L444P mutations in *GBA1* do not significantly alter the proportion of iPSC-derived DA neurons differentiating in long-term cultures. Cells differentiating from human iPSCs were fixed at 50 DIV (A-J) and 90 DIV (K-T), and then immunostained with specific antibodies against TH and MAP2. The nuclei were stained with Hoechst. The percentage of $TH^+/MAP2^+$ neurons in the cultures was 24.0-28.2% at 50 DIV (J) and 40.4-49.0% at 90 DIV (T), and this parameter was not affected by either mutation. The results are the mean (±S.E.M.) of n = 18-33 cultures per genotype from 5-6 experiments of 50 DIV cultures, or of n = 4-7 cultures per genotype for 90 DIV cultures. Scale bars: 100 µm.

Figure 3 Expression of FOXA2 and GIRK2 in iPSC-derived DA neurons from PD patients carrying the N370S or L444P *GBA1* mutation and healthy subjects. Neurons differentiating from human iPSCs were fixed at 21 DIV and immunostained with antibodies against TH and FOXA2 (A-J), or they were fixed at 54 DIV and immunostained with antibodies against TH and GIRK2 (K-T). The nuclei were stained with Hoechst and the arrows point to double positive cells, some of which are presented at high magnification in the insets. Of the TH^+ neurons, 47-53% also expressed FOXA2 (J) and 43.0-47.0% also expressed GIRK2 (T), with no effect of the mutations on these percentages. The results are the mean (±S.E.M.) of n = 3 cultures per genotype from 2-3 experiments stained with the TH and FOXA2 antibodies, or n = 6-9 cultures per genotype from 2-3 experiments stained with TH and GIRK2 antibodies. Scale bars: 10 µm.

Figure 4 N370S and L444P *GBA1* mutations affect iPSC-derived VGLUT2-DA neurons and *SLC17A6/VGLUT2* mRNA expression. (A-J) Neurons differentiating from human iPSCs were fixed at 50 DIV, and then immunostained with specific antibodies against TH and VGLUT2, labelling the nuclei with Hoechst. The arrows indicate $VGLUT2^+/TH^+$ neurons and arrowheads point to TH^+ neurons not expressing VGLUT2. (J) The percentage of TH^+ neurons expressing VGLUT2 was strongly reduced in N370S/wt and L444P/wt cultures, although the reduction was only significant in L444P/wt relative to the control cultures (**P<0.01). (K, L) Analysis of *SLC17A6*/*VGLUT2* mRNA expression by RT-qPCR on 18 DIV cultures shows significantly weaker expression in N370S/wt than in L444P/wt cultures (**P<0.01). The data was

analysed using an unpaired Student's t test to compare the mean (±SEM values) of n = 4-6 cultures from 3 experiments performed in triplicate. (M) The level of glutamate (nM/min) in the culture medium was similar in all three conditions, although it was significant higher in N370S/wt and L444P/wt cultures relative to the number of VGLUT2^{+}/TH^{+} neurons (*P<0.05; ****P<0.0001: N). The data on the cell numbers and glutamate content are the mean (±S.E.M.) of n = 5-8 cultures per genotype from 2-3 experiments. The statistical analysis was carried out using a Kruskal-Wallis test followed by a Dunn test (cell counts) or one-way ANOVA followed by a Tukey test (glutamate levels). Scale bar: 40 µm; insets, 20 µm.

Figure 5 The N370S and L444P *GBA1* mutations alter dopamine release in response to KCl. Basal (A) and KCl-evoked (B) dopamine release by iPSC-derived DA neurons into the culture medium was measured by ELISA after 44, 51 and 59 DIV, combining the results in the analysis. The data are expressed as dopamine (pg)/TH^{+} neuron (A, B) or as dopamine (pg)/TH^{+} neuron per minute (C), and presented as the mean (±S.E.M.) of n = 13-24 cultures per genotype from 3 experiments. The KCl-evoked dopamine release was significantly stronger than that of the basal dopamine release in N370S/wt and L444P/wt cultures (*P<0.05; ****P<0.0001), but this was not significantly different in the wt/wt cultures. The evoked dopamine release was significantly higher in the L444P/wt than in wt/wt cultures ($^{\#\#\#\#}$P<0.0001). Statistical analysis was performed using one-way ANOVA with a Tukey post-hoc test.

Figure 6 The N370S *GBA1* mutation increases the electrical firing rate of DA neurons. The human iPSC-derived neurons from control subjects and PD patients with N370S/wt or L444P/wt mutation in *GBA1* were maintained in culture for 90-93 days to perform electrophysiological recordings. The neurons recorded were injected with Alexa 488 and their dopaminergic phenotype was confirmed by immunostaining for TH (see supplementary Fig. S5). (A) The firing rate increased significantly in N370S/wt neurons relative to wt/wt neurons. (B) The traces illustrating spontaneous excitatory postsynaptic currents (sEPScs) are shown. The *GBA1* mutations increased, albeit not significantly, the proportion of neurons that developed sEPSCs (C) and produced no changes in their amplitude (D). However, significantly fewer sEPSCs were detected in L444P/wt neurons relatve to wt/wt neurons. The results are the mean (±S.E.M.) of n = 6-12 neurons per genotype from 2 experiments: *P<0.05; **P<0.01; ***P<0.001 (two-way ANOVA followed by a Bonferroni´s test).

Figure 7 Abundant degenerative bodies form in N370S and L444P *GBA1* mutant neurons. (A, C, and E) Low-magnification micrographs from 103 DIV cultures of iPSC-derived neurons from control healthy subjects (A) and from patients carrying the N370S/wt (C) or the L444P/wt (E) *GBA1* mutations. Note that mutant neurons contain large structures that resemble degenerative bodies (arrows in C and E). (B, D and F) Micrographs of degenerative bodies at higher magnification. (B) This cell derived from a control subject contain a few autophagosome-like vacuoles. The large degenerative body-like structures found in patient-derived neurons carrying the N370S/wt (D) or the L444P/wt (F)

mutation are full of vacuoles resembling autophagosomes and dysfunctional lysosomes. Scale Bars: A, C, E, 5 μm; B, D, F, 1 μm.

Figure 8 The N370S and L444P *GBA1* mutations promote multilamellar body formation in iPSC-derived neurons. (A-C) Multilamellar bodies (MLBs) in cultured iPSC-derived neurons from patients carrying the N370S/wt *GBA1* mutation. The membranes that integrate these structures are clearly disorganized. (D) Low magnification micrograph showing a cultured iPSC-derived neuron from a patient carrying the L4444P/wt *GBA1* mutation. The boxed area is shown at higher magnification in (E). This cell contains an 'atypical' structure of membrane cisternae arranged in a semi-circular manner. Note the electron-dense material located among the cisternae. (F-H) Multilamellar structures in cultured iPSC-derived neurons from patients carrying the L444P/wt *GBA1* mutation. The membrane cisternae that integrate the structures in F and G are perfectly distinguishable. Note that these multilamellar structures enclose cytoplasmic remnants with heterogeneous material. The membranes that integrate the structure shown in H are disorganized. Scale Bars: A-C, E-H, 500 nm; D, 5 μm.

Figure 9 The N370S and L444P *GBA1* mutations alter the Golgi apparatus of iPSC-derived neurons. (A) Golgi apparatus (GA) dictyosomes have a normal appearance in iPSC-derived neurons from control healthy subjects. (B-F) A large number of GA dictyosomes with an abnormal and vacuolated appearance was found in iPSC-derived neurons from patients carrying the

N370S/wt (B, C) or L444P/wt *GBA1* mutation (D-F). The dictyosomes in the boxed areas in D are shown at higher magnification in E and F. Note that these dictyosomes are completely vacuolated. (G) Graph depicting the proportion of vacuolated and non-vacuolated dictyosomes in iPSC-derived neurons from controls and from patients carrying the N370S/wt or L444P/wt *GBA1* mutation. Scale Bars: A, 4 µm; B, C, 500 nm; D, E, F, 250 nm.

Figure 10 The N370S *GBA1* mutation augments the α-synuclein aggregates in cell bodies and dendrites of DA neurons. (A-L, N-Y) Human iPSC-derived neurons from control subjects and PD patients carrying N370S/wt or L444P/wt mutations in *GBA1* were maintained in culture for 95 or 103 days and then immunostained for TH, MAP2 and α-synuclein. The aggregates in the soma (M) and dendrites (Z) of TH^+ neurons were semi-automatically counted using ImageJ after tracing the neuron and setting the thresholds. Arrows point to examples of aggregates. The results are the mean (±S.E.M.) of n = >40 neurons per genotype from 3 experiments and they are expressed as the number of aggregates per soma or per dendritic area. There were significantly more α-synuclein aggregates in the cell bodies and dendrites of N370S/wt *GBA1*-DA neurons than in wt/wt and L444P/wt neurons: **P<0.01; ***P<0.001; ****P<0.0001 (Kruskal-Wallis test followed by Dunn´s multiple comparisons test). There was a trend towards more α-synuclein in the culture medium in N370S/wt *GBA1*-cultures, albeit not significant (Z'). Scale bar: 8 µm.

Figure 11 The N370S *GBA1* mutation increases CRYAB expression in DA neurons. (A-I) Human iPSC-derived cells from control subjects and PD patients

carrying N370S/wt or L444P/wt mutations in *GBA1* were maintained in culture for 30 days and then immunostained for TH and CRYAB. (J) There was a marked increase in the DA neurons expressing CRYAB in the N370S/wt cultures relative to the controls (****P<0.0001), while the increase in L444P/wt cultures was not statistically significant. The arrows indicate $CRYAB^+/TH^+$ neurons and the results are the mean (±S.E.M.) of n = 6-8 cultures per genotype from 2-3 experiments. The statistical analysis was carried out using one-way ANOVA followed by Games-Howell's post-hoc test. (K, L) Analysis of *CRYAB* mRNA expression by RT-qPCR in samples of 18 DIV cultures. A significant increase in *CRYAB* expression was found in N370S/wt cultures relative to the controls (**P<0.01) and to the L444P/wt cultures (*P<0.05). The statistical analysis was carried out using an unpaired Student's t test with Welch correction to compare the mean (±S.E.M.) values of n = 4-6 cultures from 3 experiments. Scale bar: 10 µm.

Figure 12 *VGLUT2* and *CRYAB* mRNA expression is enhanced in the post-mortem Substantia Nigra of PD patients. Gene expression analysed by RT-qPCR in samples from the substantia nigra (A) and hippocampal cortex (B) reveals a significant increase of *SLC17A6/VGLUT2* and *CRYAB* mRNA expression in the substantia nigra of PD patients (*P<0.05). The violin plots represent the density, distribution and the median of the data obtained by analysing samples from 4 controls and 4 PD patients carrying no *GBA1* mutations, performed in triplicate. The statistical analysis was carried out using an unpaired Student's t test (*SLC17A6/VGLUT2*) applying Welch's correction (*CRYAB*) to compare the mean (±S.E.M.) values.

Figure 1

A

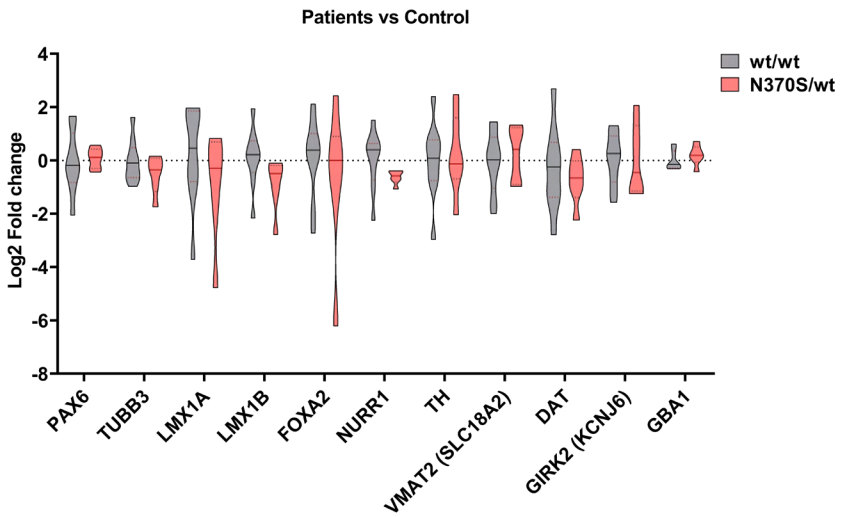
Patients vs Control
wt/wt
N370S/wt
Log2 Fold change
4
2
0
-2
-4
-6
-8
PAX6
TUBB3
LMX1A
LMX1B
FOXA2
NURR1
TH
VMAT2 (SLC18A2)
DAT
GIRK2 (KCNJ6)
GBA1

B

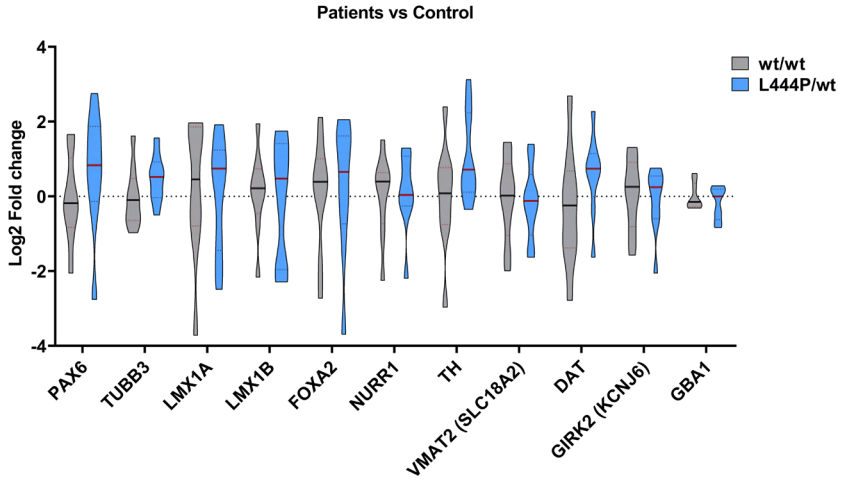
Patients vs Control
wt/wt
L444P/wt
Log2 Fold change
4
2
0
-2
-4
PAX6
TUBB3
LMX1A
LMX1B
FOXA2
NURR1
TH
VMAT2 (SLC18A2)
DAT
GIRK2 (KCNJ6)
GBA1

C

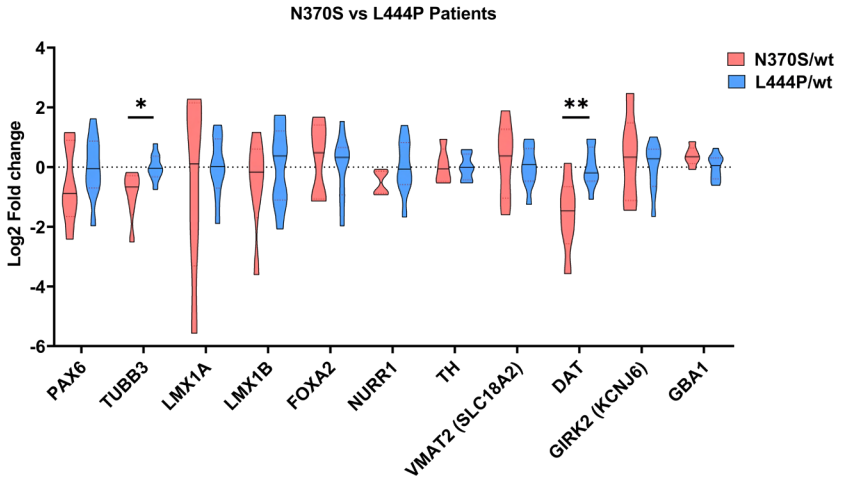
N370S vs L444P Patients
N370S/wt
L444P/wt
Log2 Fold change
4
2
0
-2
-4
-6
*
**
PAX6
TUBB3
LMX1A
LMX1B
FOXA2
NURR1
TH
VMAT2 (SLC18A2)
DAT
GIRK2 (KCNJ6)
GBA1

Figure 2

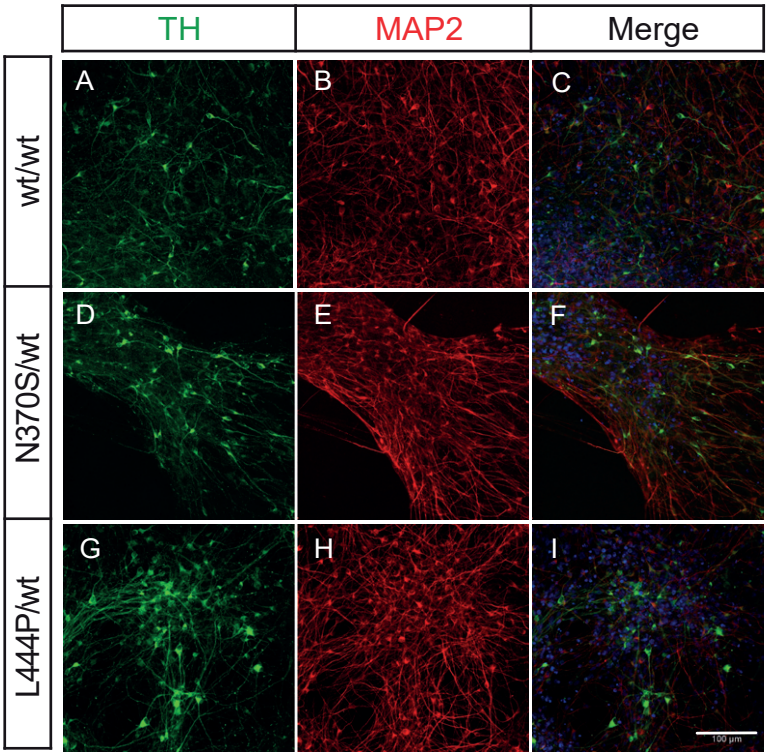
TH
MAP2
Merge
wt/wt
N370S/wt
L444P/wt
A
B
C
D
E
F
G
H
I
100 µm

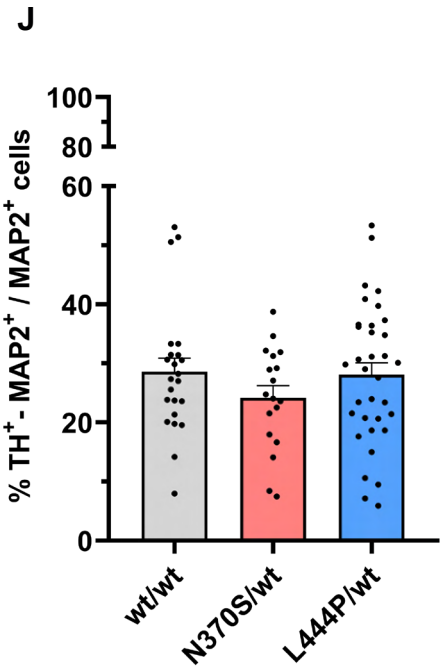
J
% TH+- MAP2+ / MAP2+ cells
100
80
60
40
20
0
wt/wt
N370S/wt
L444P/wt

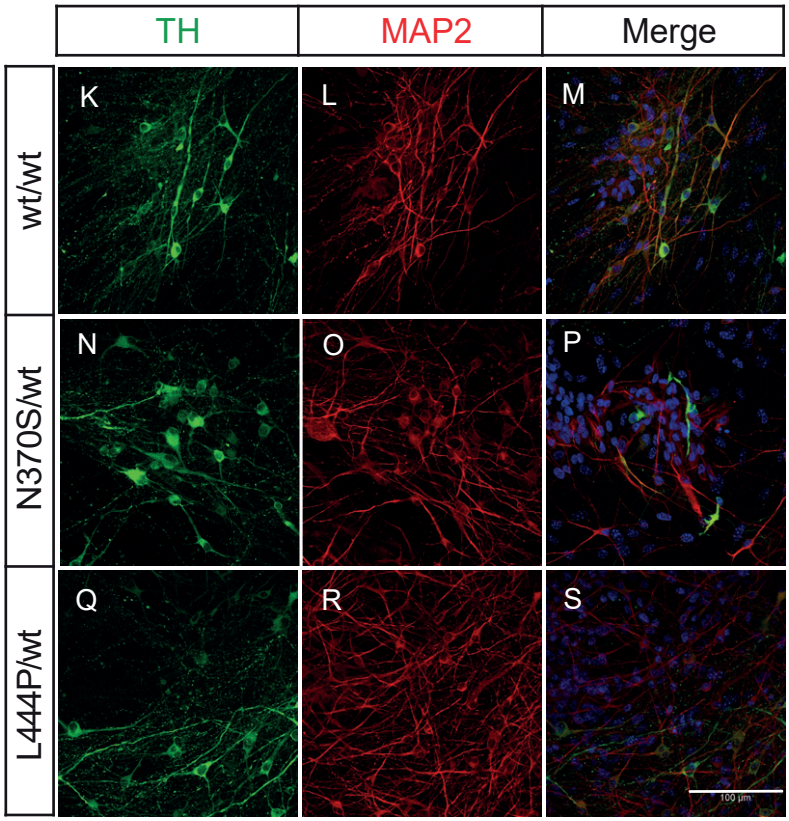
TH
MAP2
Merge
wt/wt
N370S/wt
L444P/wt
K
L
M
N
O
P
Q
R
S
100 µm

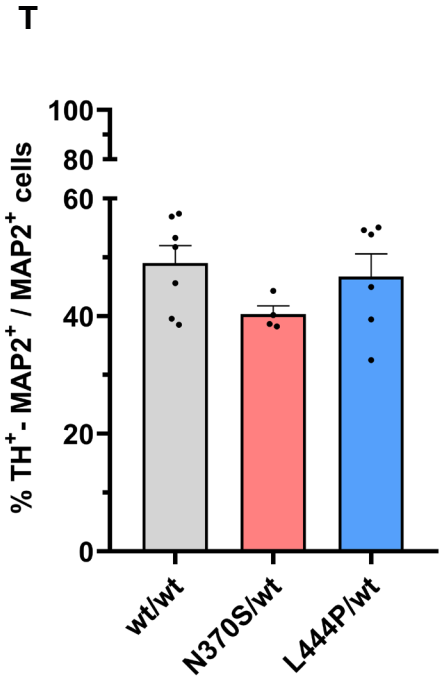
T
% TH+- MAP2+ / MAP2+ cells
100
80
60
40
20
0
wt/wt
N370S/wt
L444P/wt

Figure 3

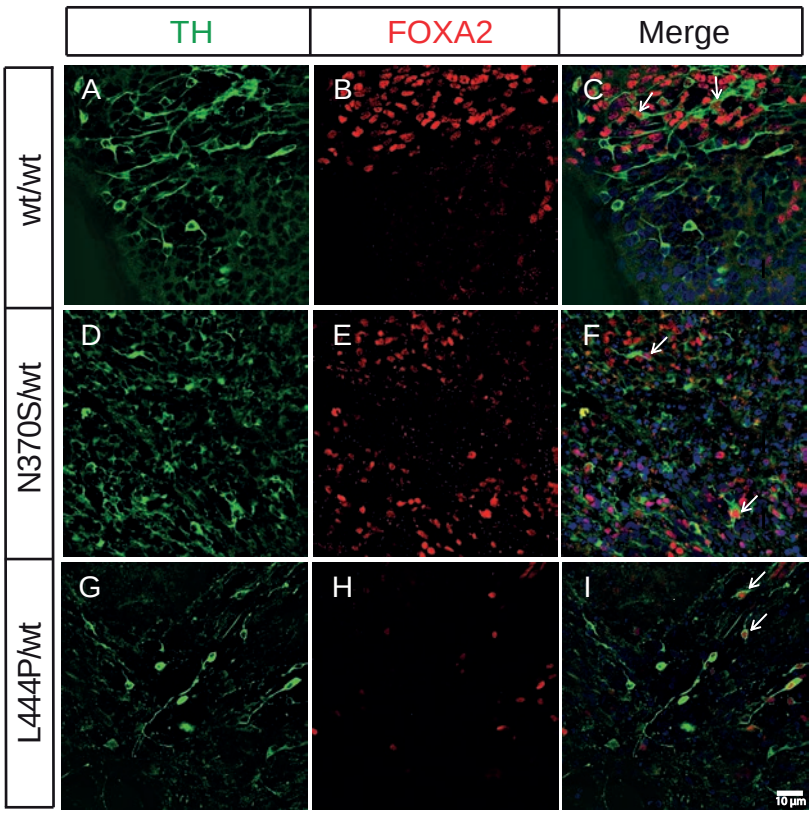
TH
FOXA2
Merge
wt/wt
N370S/wt
L444P/wt
A
B
C
D
E
F
G
H
I
10 µm

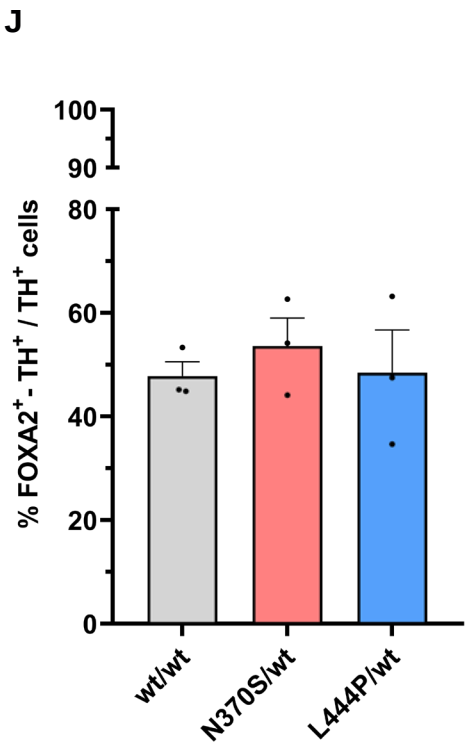
J
% FOXA2+ - TH+ / TH+ cells
100
90
80
60
40
20
0
wt/wt
N370S/wt
L444P/wt

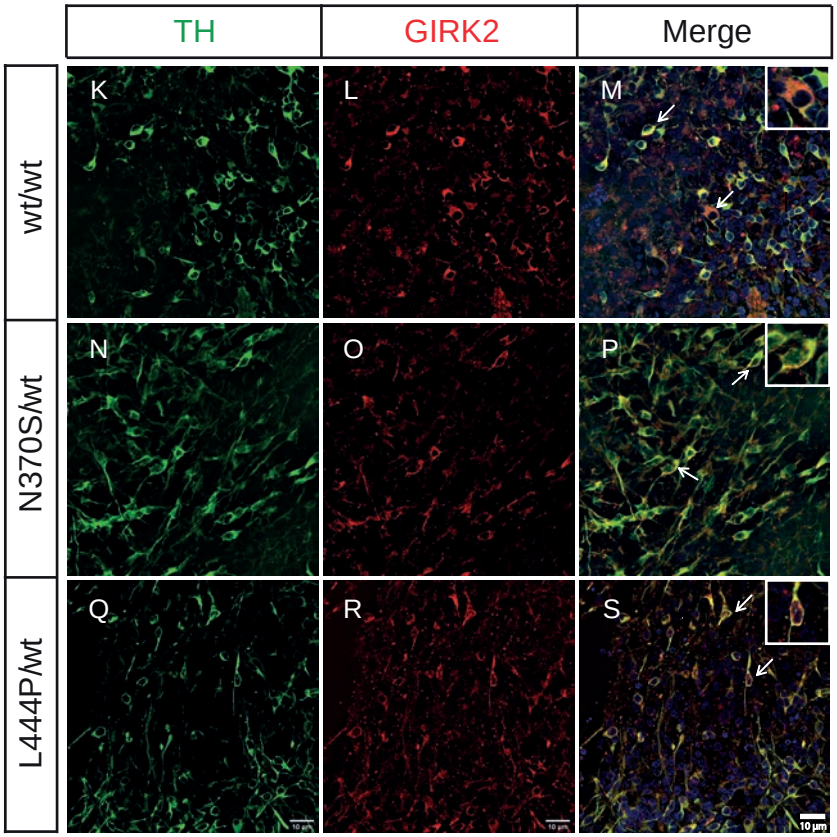
TH
GIRK2
Merge
wt/wt
N370S/wt
L444P/wt
K
L
M
N
O
P
Q
R
S
10 µm

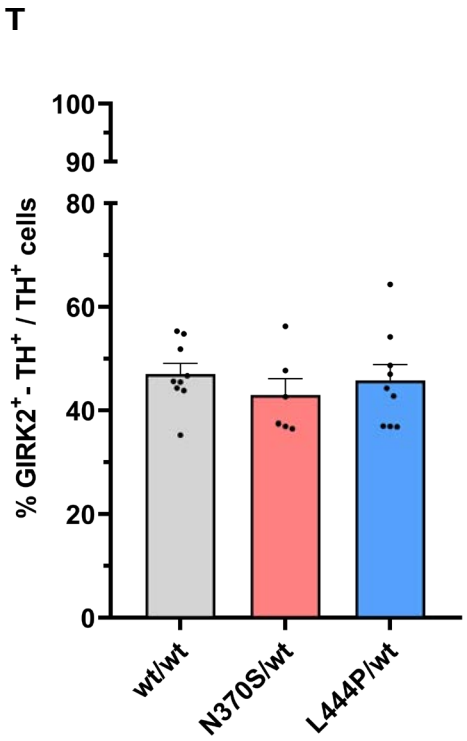
T
% GIRK2+ - TH+ / TH+ cells
100
90
80
60
40
20
0
wt/wt
N370S/wt
L444P/wt

Figure 4

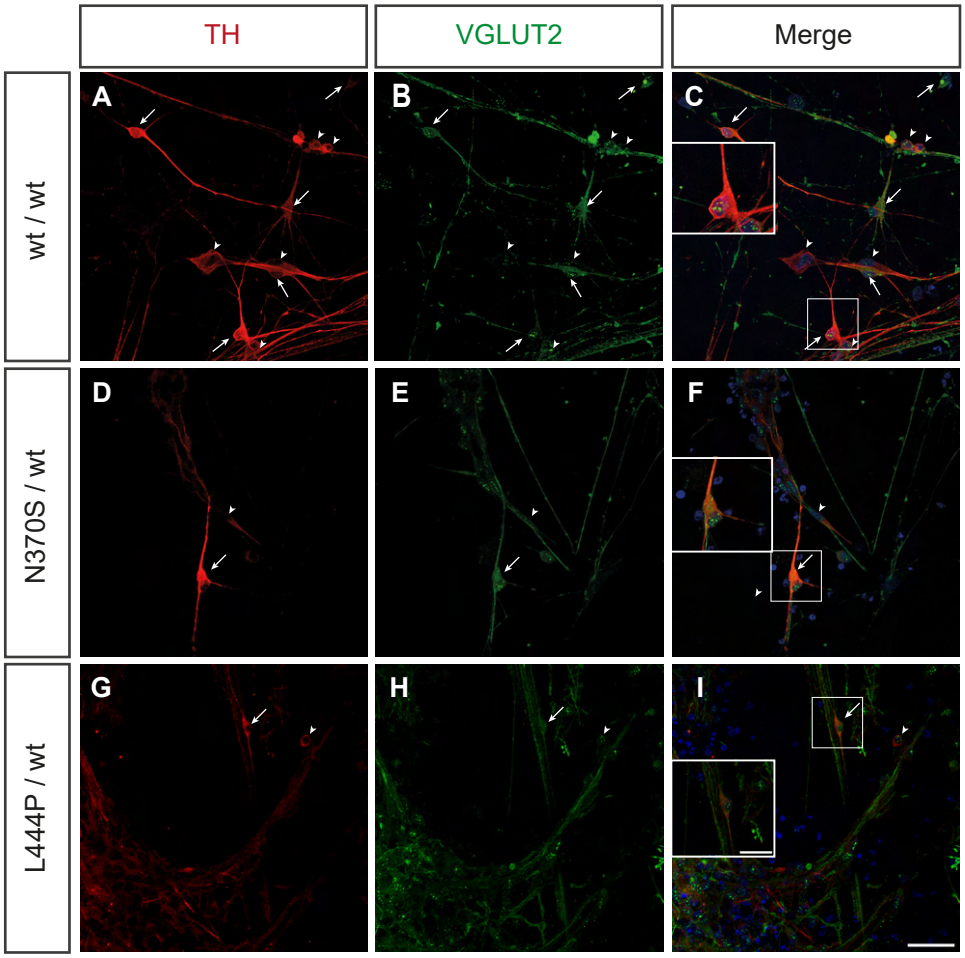
TH
VGLUT2
Merge
wt / wt
N370S / wt
L444P / wt
A
B
C
D
E
F
G
H
I

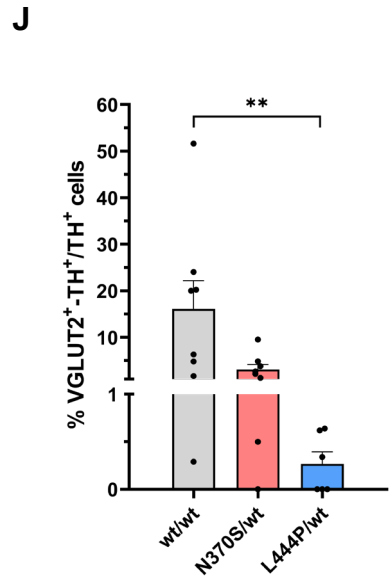
J
% VGLUT2+-TH+/TH+ cells
**
wt/wt
N370S/wt
L444P/wt

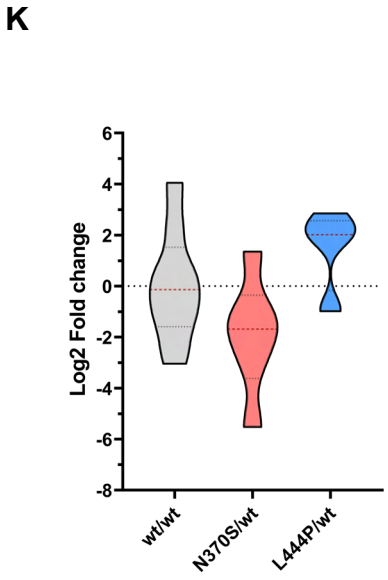
K
Log2 Fold change
wt/wt
N370S/wt
L444P/wt

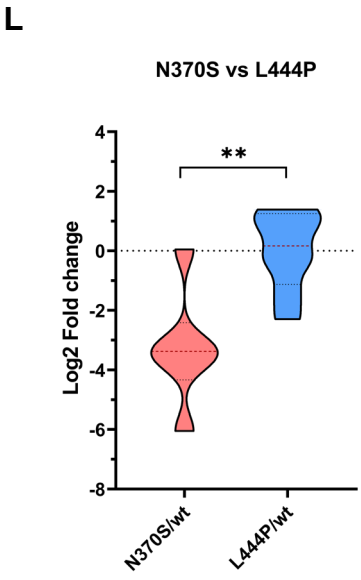
L
N370S vs L444P
Log2 Fold change
**
N370S/wt
L444P/wt

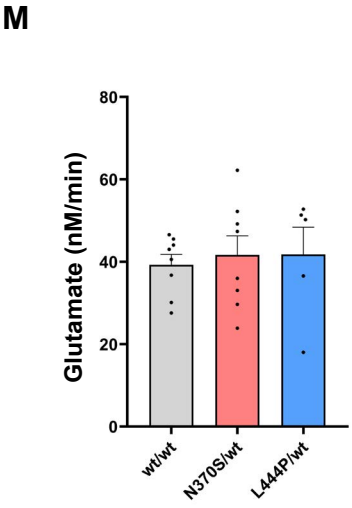
M
Glutamate (nM/min)
wt/wt
N370S/wt
L444P/wt

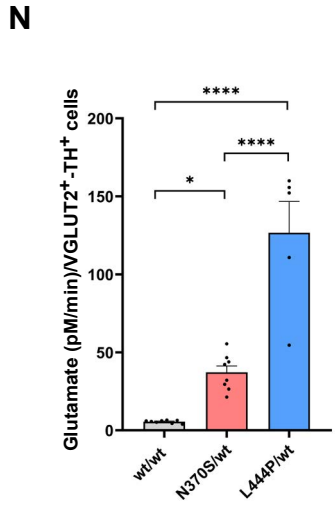
N
Glutamate (pM/min)/VGLUT2+-TH+ cells
****
****
*
wt/wt
N370S/wt
L444P/wt

Figure 5

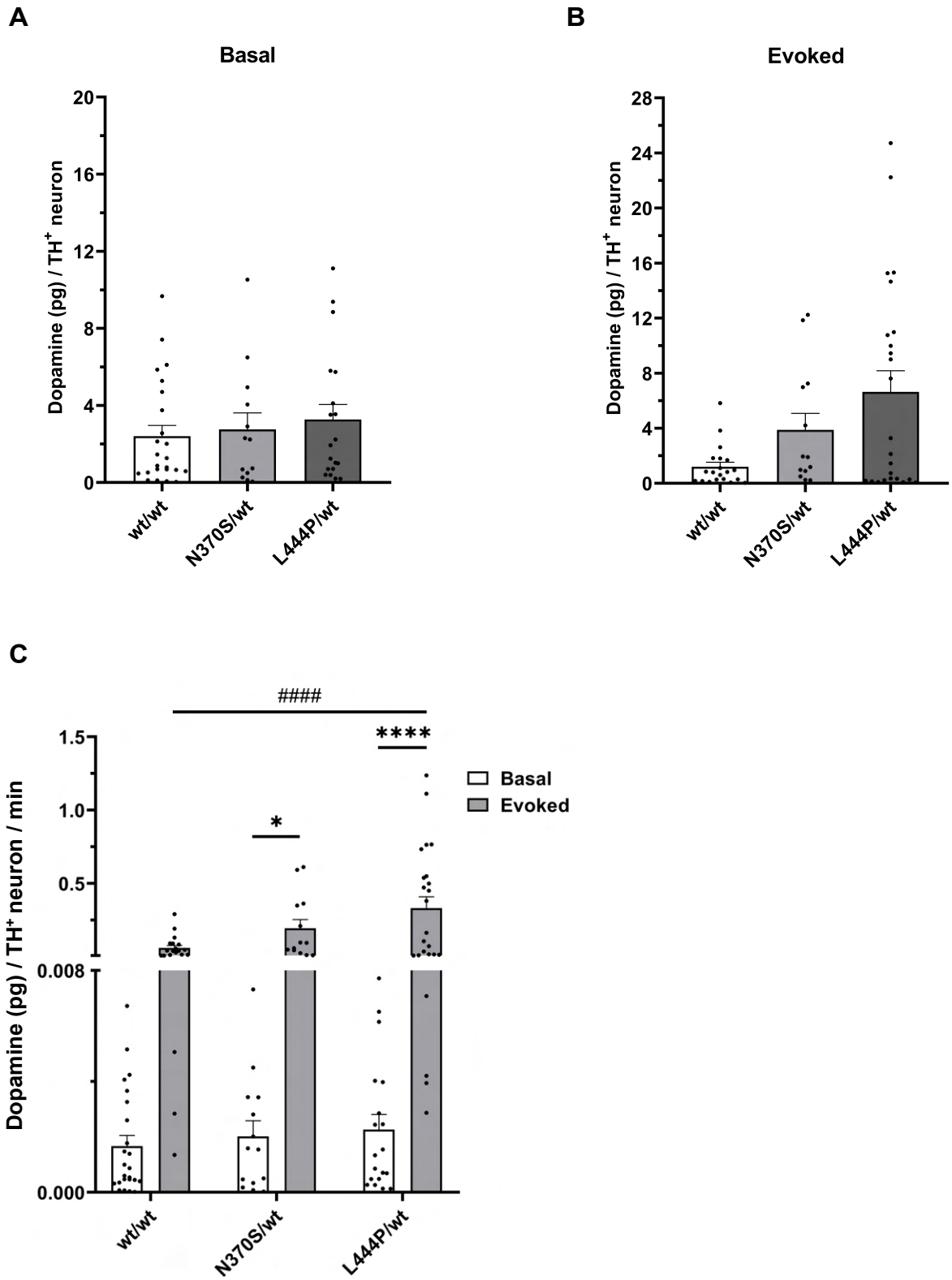
A
Basal
Dopamine (pg) / TH+ neuron
20
16
12
8
4
0
wt/wt
N370S/wt
L444P/wt
B
Evoked
Dopamine (pg) / TH+ neuron
28
24
20
16
12
8
4
0
wt/wt
N370S/wt
L444P/wt
C
Dopamine (pg) / TH+ neuron / min
1.5
1.0
0.5
0.008
0.000
####
****
*
Basal
Evoked
wt/wt
N370S/wt
L444P/wt

Figure 6

A Firing rate

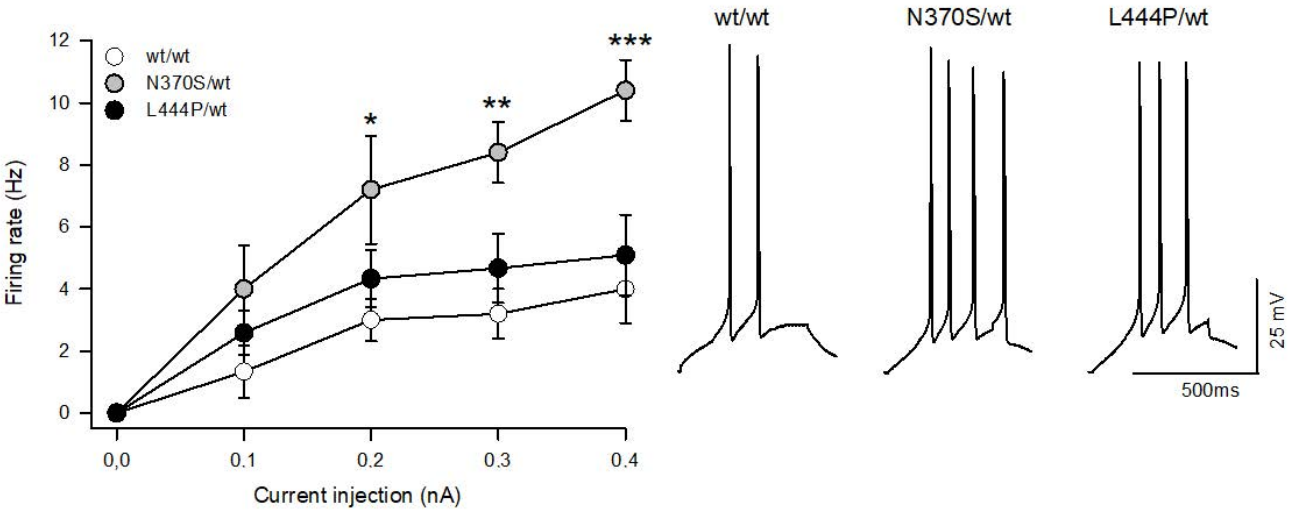

B sEPSCs

C

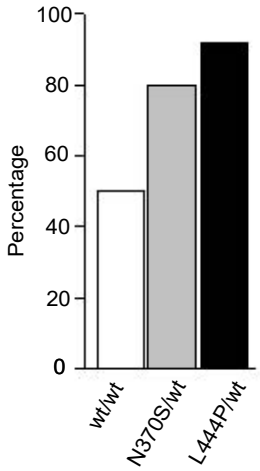

D

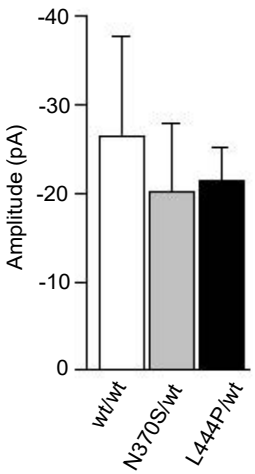

E

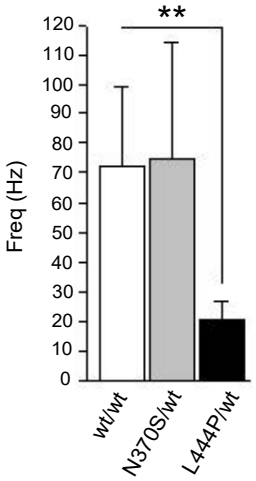

Figure 7

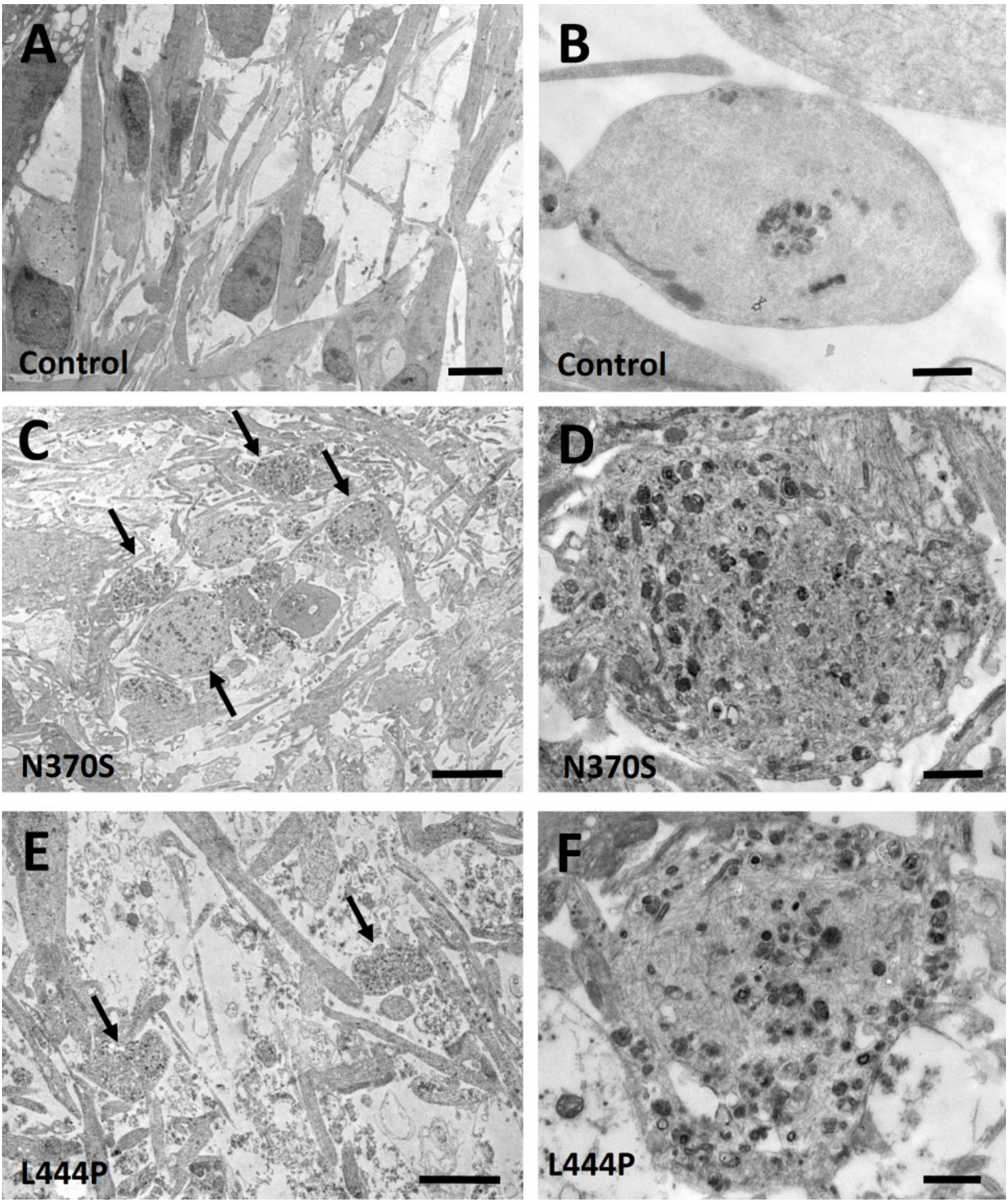

Figure 8

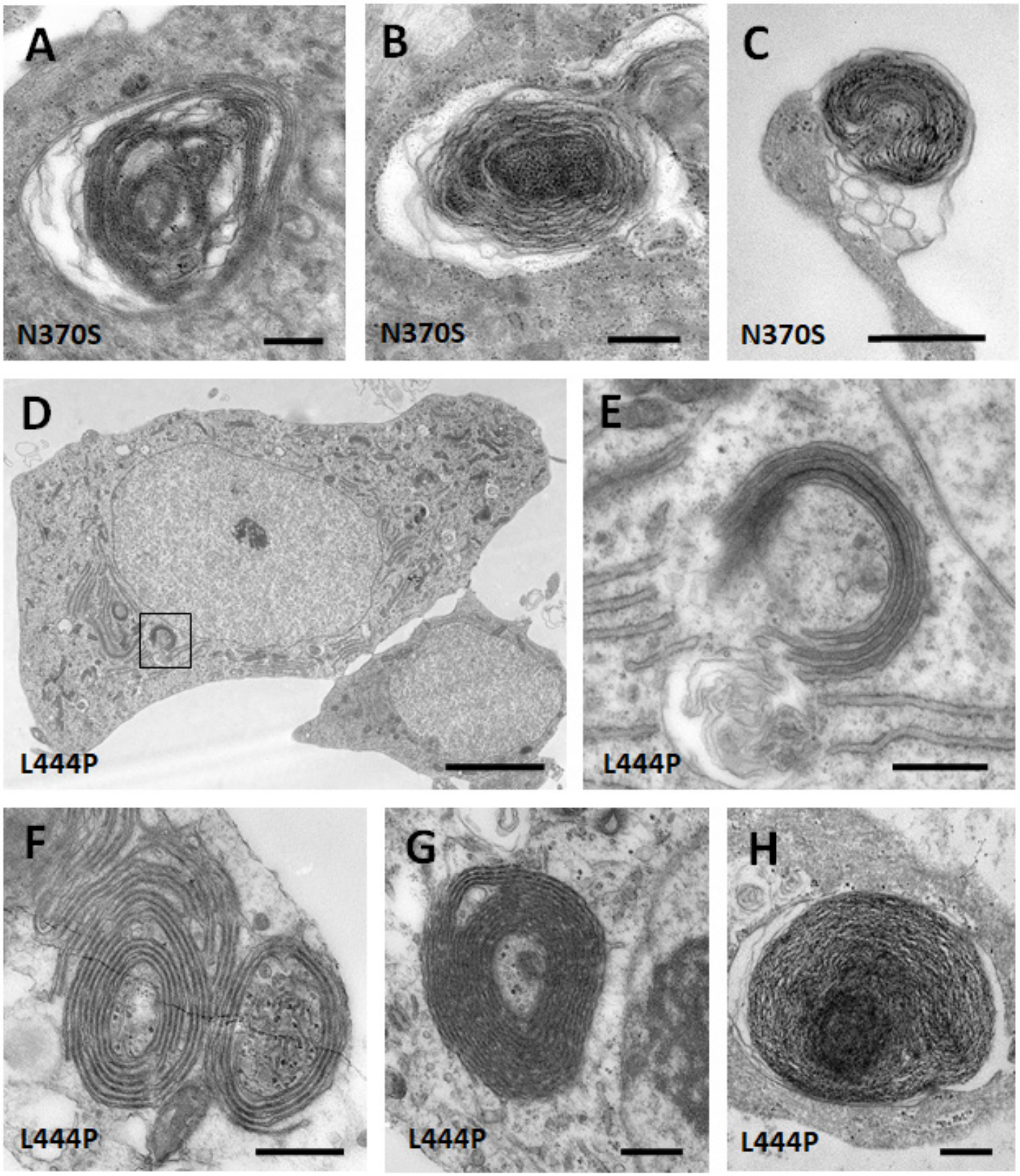

Figure 9

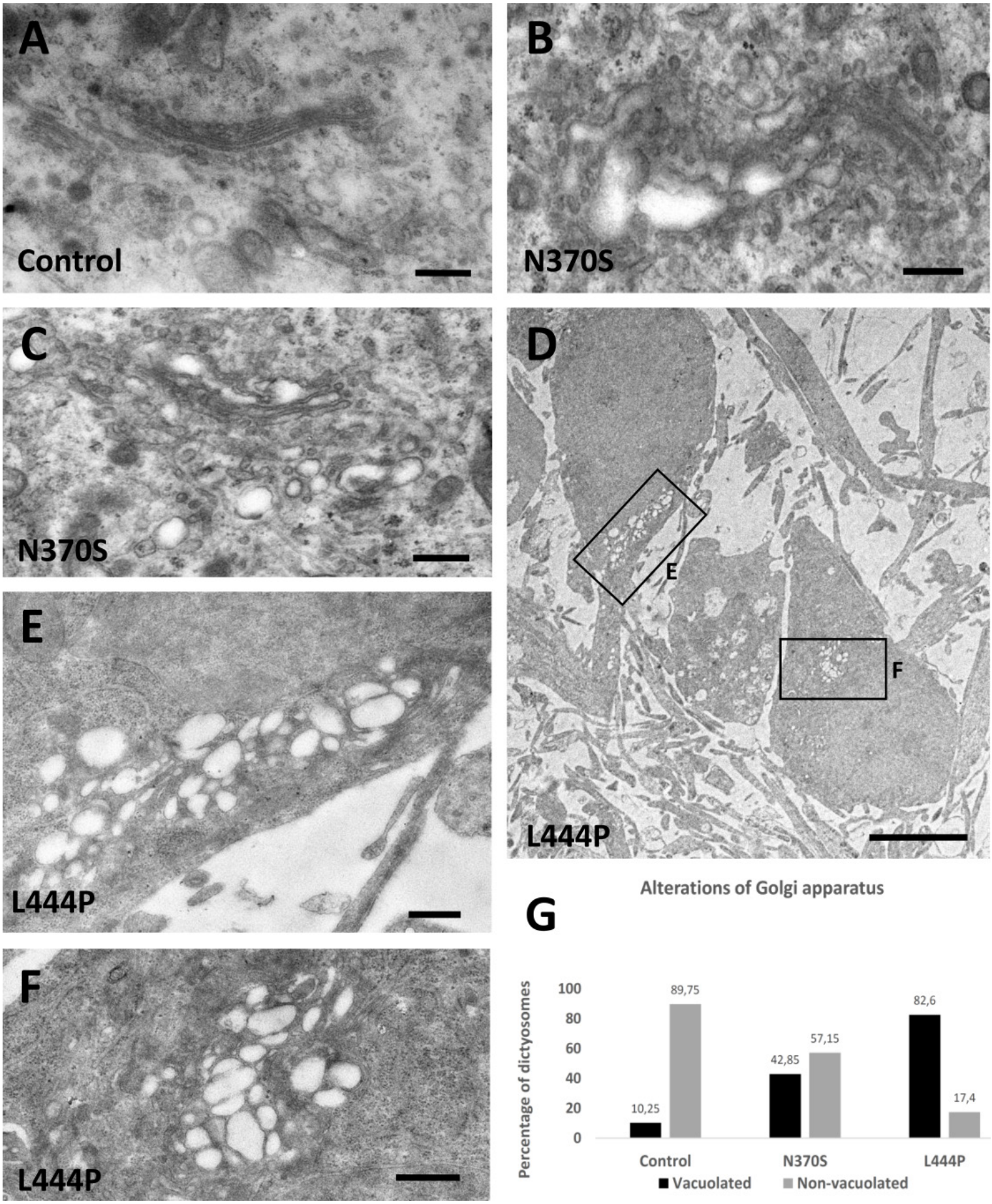
A
Control
B
N370S
C
N370S
D
E
F
L444P
E
L444P
F
L444P
G
Alterations of Golgi apparatus
Percentage of dictyosomes
100
80
60
40
20
0
10,25
89,75
42,85
57,15
82,6
17,4
Control
N370S
L444P
Vacuolated
Non-vacuolated

Figure 10

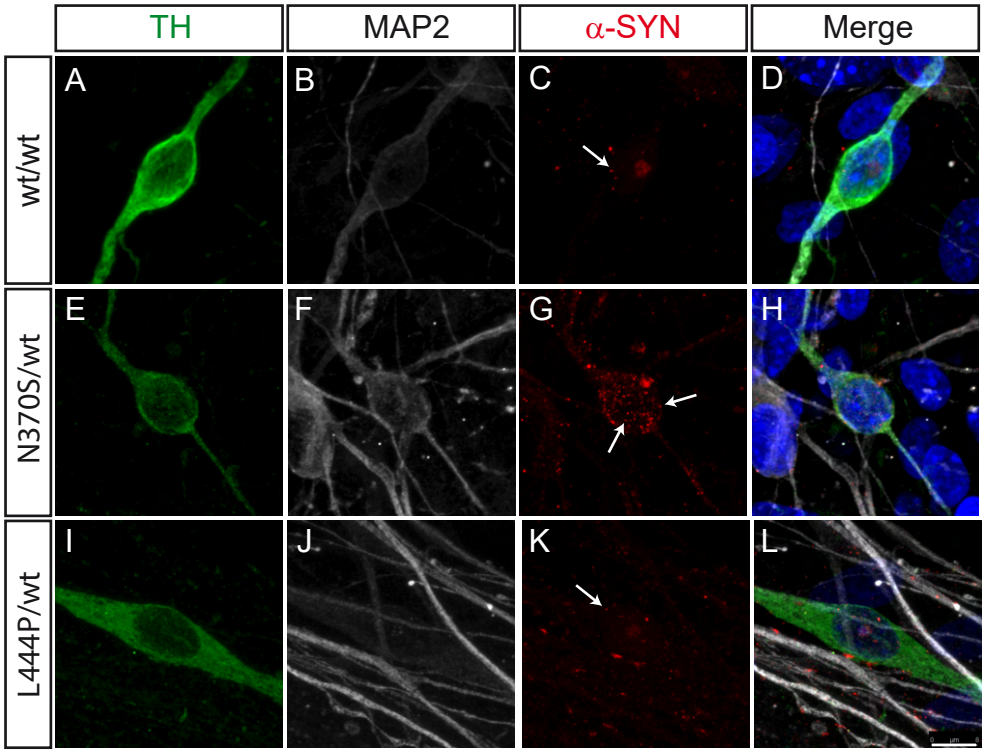
TH
MAP2
α-SYN
Merge
wt/wt
N370S/wt
L444P/wt
A
B
C
D
E
F
G
H
I
J
K
L

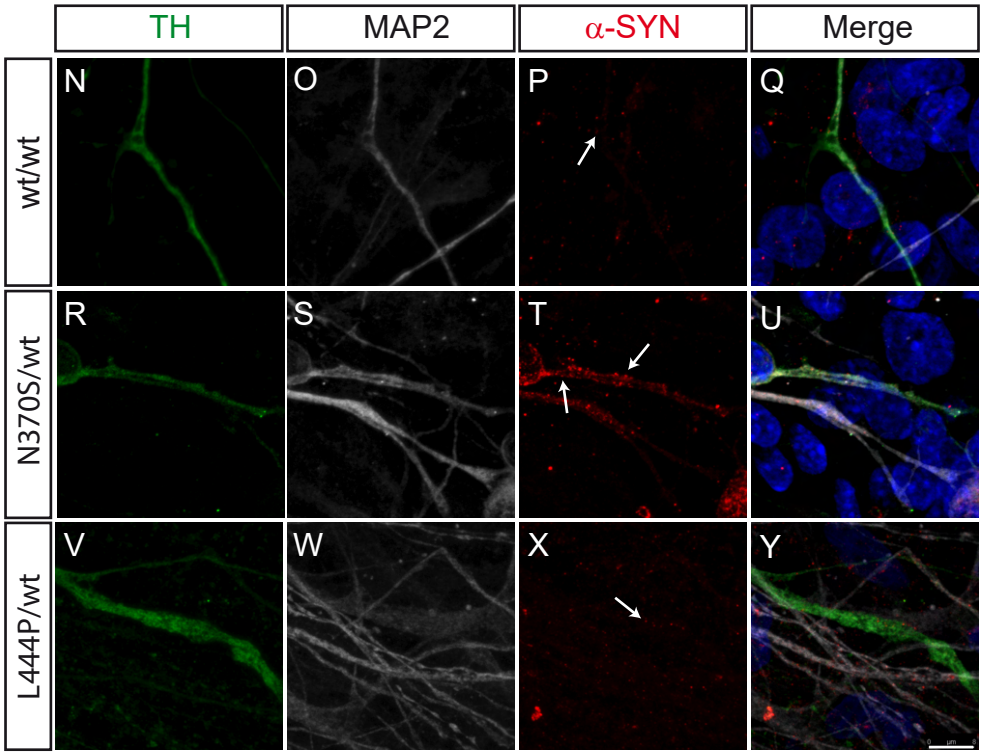
TH
MAP2
α-SYN
Merge
wt/wt
N370S/wt
L444P/wt
N
O
P
Q
R
S
T
U
V
W
X
Y

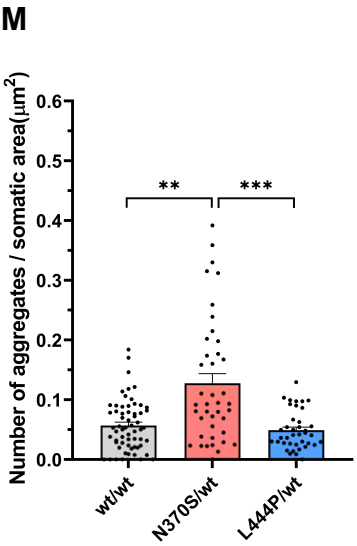
M
Number of aggregates / somatic area(μm²)
0.0
0.1
0.2
0.3
0.4
0.5
0.6
**
***
wt/wt
N370S/wt
L444P/wt

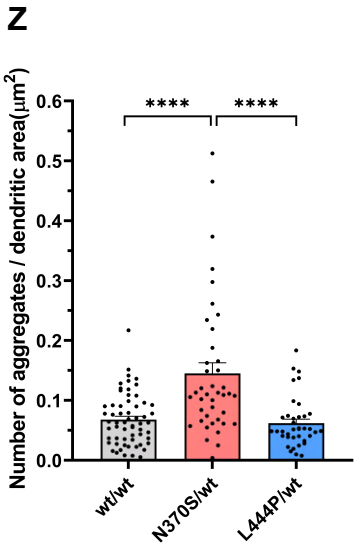
Z
Number of aggregates / dendritic area(μm²)
0.0
0.1
0.2
0.3
0.4
0.5
0.6
****
****
wt/wt
N370S/wt
L444P/wt

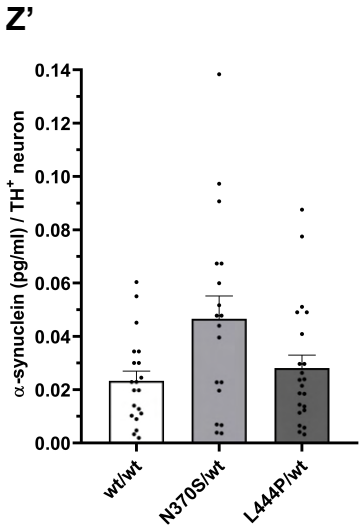
Z'
α-synuclein (pg/ml) / TH⁺ neuron
0.00
0.02
0.04
0.06
0.08
0.10
0.12
0.14
wt/wt
N370S/wt
L444P/wt

Figure 11

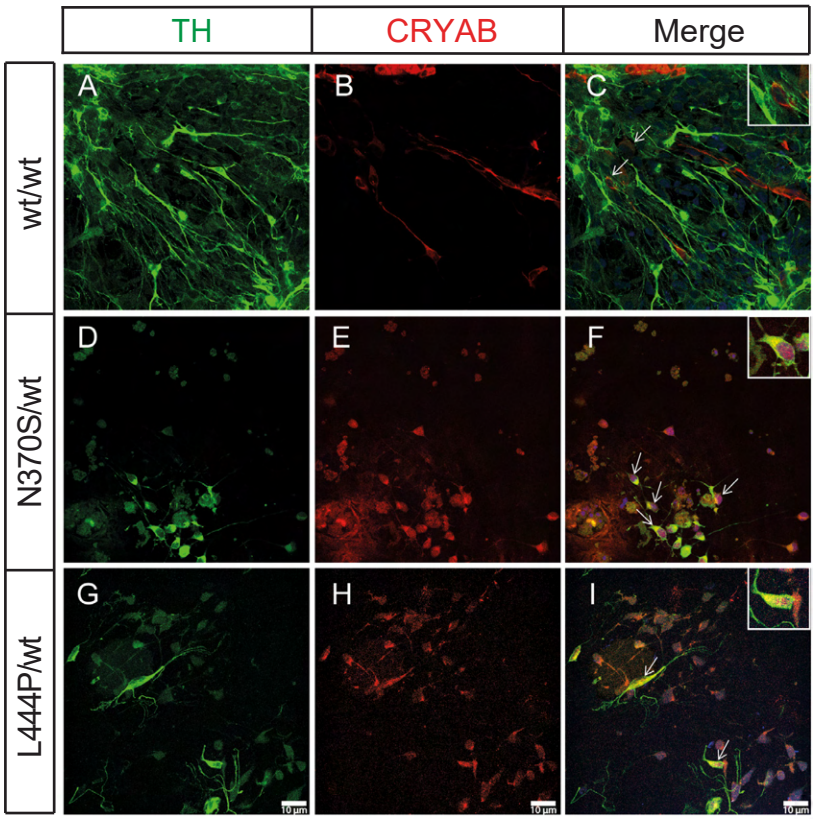
TH
CRYAB
Merge
wt/wt
N370S/wt
L444P/wt
A
B
C
D
E
F
G
H
I
10 µm

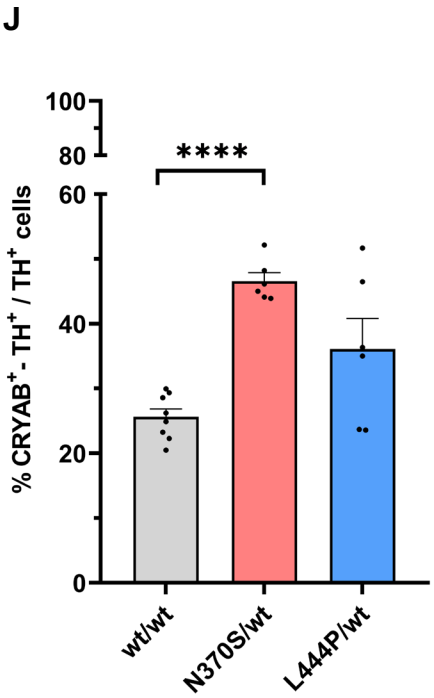
J
% CRYAB+ - TH+ / TH+ cells
100
80
60
40
20
0
****
wt/wt
N370S/wt
L444P/wt

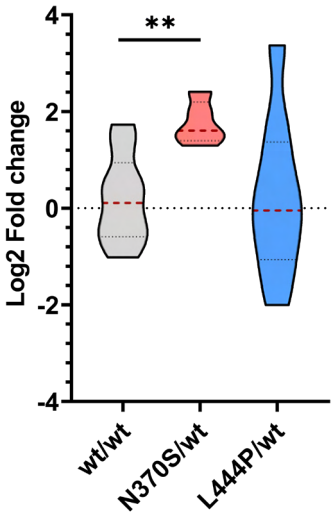
K
Mutations vs wt/wt
Log2 Fold change
4
2
0
-2
-4
**
wt/wt
N370S/wt
L444P/wt

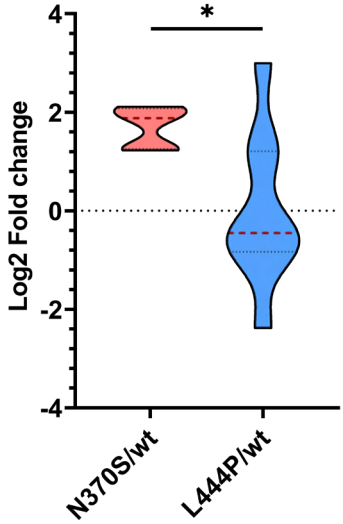
L
N370S vs L444P
Log2 Fold change
4
2
0
-2
-4
*
N370S/wt
L444P/wt

Figure 12

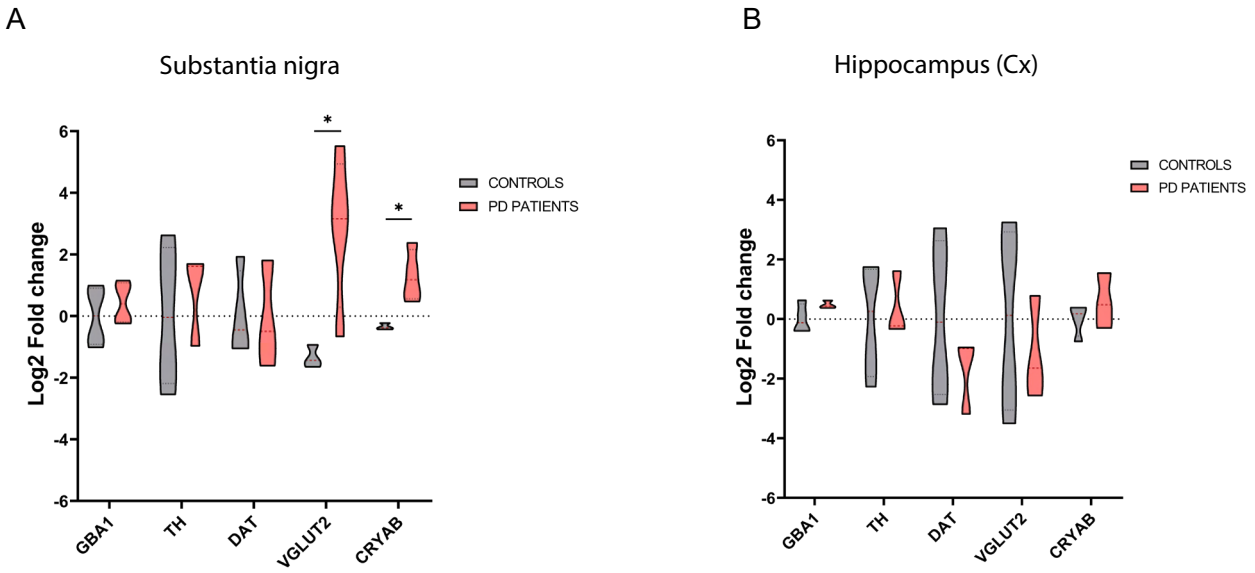
A
Substantia nigra
Log2 Fold change
6
4
2
0
-2
-4
-6
*
*
GBA1
TH
DAT
VGLUT2
CRYAB
CONTROLS
PD PATIENTS
B
Hippocampus (Cx)
Log2 Fold change
6
4
2
0
-2
-4
-6
GBA1
TH
DAT
VGLUT2
CRYAB
CONTROLS
PD PATIENTS